Cell Reports

Article

Obesity-induced astrocyte dysfunction impairs heterosynaptic plasticity in the orbitofrontal cortex

Graphical abstract

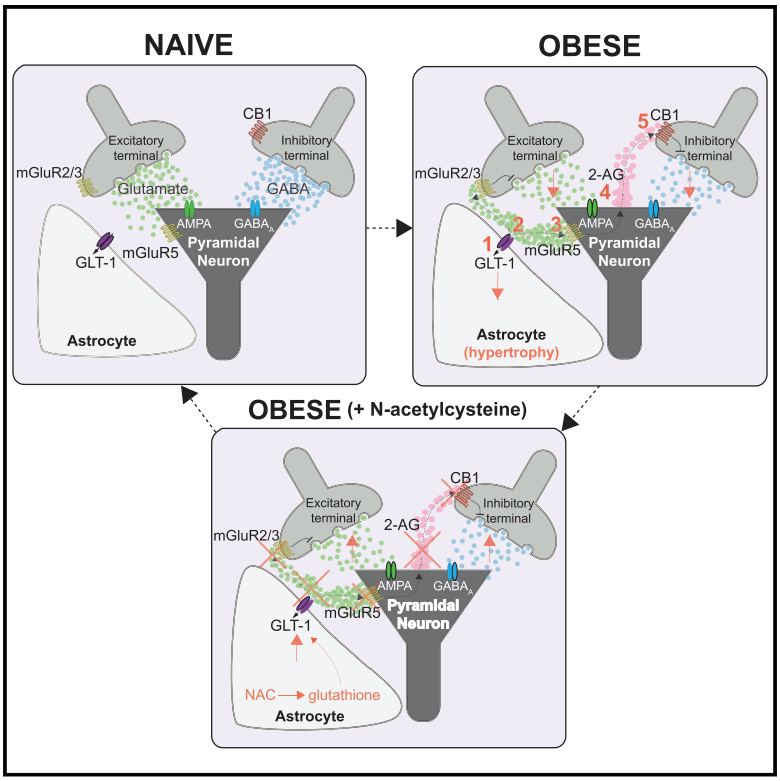

Authors

Benjamin K. Lau, Ciaran Murphy-Royal, Manpreet Kaur, Min Qiao, Jaideep S. Bains, Grant R. Gordon, Stephanie L. Borgland

Correspondence

s.borgland@ucalgary.ca

In brief

Lau et al. find that obesity disrupts orbitofrontal cortex function, a region involved in updating value-related information about food. They find that an obesogenic diet impairs glutamate transport in astrocytes, leading to a cascade of events that disrupt inhibitory synaptic plasticity. These alterations are reversed with a dietary supplement, N-acetylcysteine.

Highlights

- Obesity induces astrocyte hypertrophy and disrupts glutamate transport
- Impaired glutamate homeostasis drives endocannabinoid synthesis
- Elevated endocannabinoids induce a long-term depression of GABA transmission
- NAC restores astrocytic glutamate transport, which rescues the synaptic deficits

Lau et al., 2021, Cell Reports *36*, 109563
August 17, 2021
https://doi.org/10.1016/j.celrep.2021.109563

CellPress

Cell Reports

CellPress
OPEN ACCESS

Article

Obesity-induced astrocyte dysfunction impairs heterosynaptic plasticity in the orbitofrontal cortex

Benjamin K. Lau,[1] Ciaran Murphy-Royal,[1] Manpreet Kaur,[1] Min Qiao,[1] Jaideep S. Bains,[1] Grant R. Gordon,[1] and Stephanie L. Borgland[1,2,*]

[1]Department of Physiology and Pharmacology, Hotchkiss Brain Institute, The University of Calgary, 3330 Hospital Dr. NW, Calgary, Alberta T2N 4N1, Canada

[2]Lead contact

*Correspondence: s.borgland@ucalgary.ca

https://doi.org/10.1016/j.celrep.2021.109563

SUMMARY

Overconsumption of highly palatable, energy-dense food is considered a key driver of the obesity pandemic. The orbitofrontal cortex (OFC) is critical for reward valuation of gustatory signals, yet how the OFC adapts to obesogenic diets is poorly understood. Here, we show that extended access to a cafeteria diet impairs astrocyte glutamate clearance, which leads to a heterosynaptic depression of GABA transmission onto pyramidal neurons of the OFC. This decrease in GABA tone is due to an increase in extrasynaptic glutamate, which acts via metabotropic glutamate receptors to liberate endocannabinoids. This impairs the induction of endocannabinoid-mediated long-term plasticity. The nutritional supplement, N-acetylcysteine rescues this cascade of synaptic impairments by restoring astrocytic glutamate transport. Together, our findings indicate that obesity targets astrocytes to disrupt the delicate balance between excitatory and inhibitory transmission in the OFC.

INTRODUCTION

Obesity is characterized by a disruption in energy balance, in which intake of energy exceeds its output (Spiegelman and Flier, 2001). A key contributor to excess energy intake is overeating, driven by an abundance of palatable, hypercaloric food. Furthermore, once obesity is established it is persistent, such that weight loss is rarely maintained (Hall and Guo, 2017). A hypothesis underlying the persisting effects of obesity is that plasticity occurs in neural circuits, leading animals to defend elevated body weight (Matikainen-Ankney and Kravitz, 2018). Neural plasticity associated with feeding regulation, energy homeostasis, and obesity has been well characterized within hypothalamic and mesolimbic systems (Matikainen-Ankney and Kravitz, 2018; Thoeni et al., 2020). However, there is growing evidence implicating cortical systems involved in decision-making and response inhibition (Lowe et al., 2019; Seabrook and Borgland, 2020). The orbitofrontal cortex (OFC) processes food-related signals (Jennings et al., 2019; Seabrook and Borgland, 2020). By integrating afferent and efferent projections from sensory, limbic, and prelimbic regions (Ongür and Price, 2000), the OFC guides decision-making associated with food intake, such as processing relative value and updating actions based on current energy status (Seabrook and Borgland, 2020). However, less is known about how obesogenic diets influence plasticity in cortical regions.

One of the hallmarks of obesity is inflammation and astrocyte reactivity in the brain. Following short- and long-term exposure to an obesogenic diet, astrocytes undergo morphological and functional changes leading to a hypertrophic and/or reactive phenotype associated with an inflammatory response (Douglass et al., 2017; García-Cáceres et al., 2013). However, the underlying mechanisms linking obesity-induced changes in astrocytes to neuronal plasticity are not well understood. Under physiological conditions, astrocytes provide metabolic support to maintain neuronal synaptic function. Forming part of a tripartite synapse, astrocytes can regulate synaptic transmission through the uptake of neurotransmitters in the synaptic cleft (Chen et al., 2019; Hirase et al., 2014). In particular, astrocytes specifically express glutamate transporter 1 (GLT-1), responsible for the predominant clearance of glutamate in the brain (Tanaka et al., 1997). Although there is some evidence in other regions indicating obesity-induced changes in GLT-1 levels (Linehan et al., 2018; Tsai et al., 2018), the functional consequences of altered astrocytic glutamate transport on downstream neurotransmitter systems is lacking.

Using a diet known to produce reward dysfunction and overeating (Johnson and Kenny, 2010), we demonstrated that an obesogenic diet influences spine density and suppresses GABAergic synaptic transmission in the lateral OFC (lOFC) (Thompson et al., 2017). However, the mechanisms underlying these synaptic changes are unknown. We hypothesize that overnutrition with palatable food readily available for human consumption alters heterosynaptic plasticity in the OFC via a neuron-astrocyte interaction.

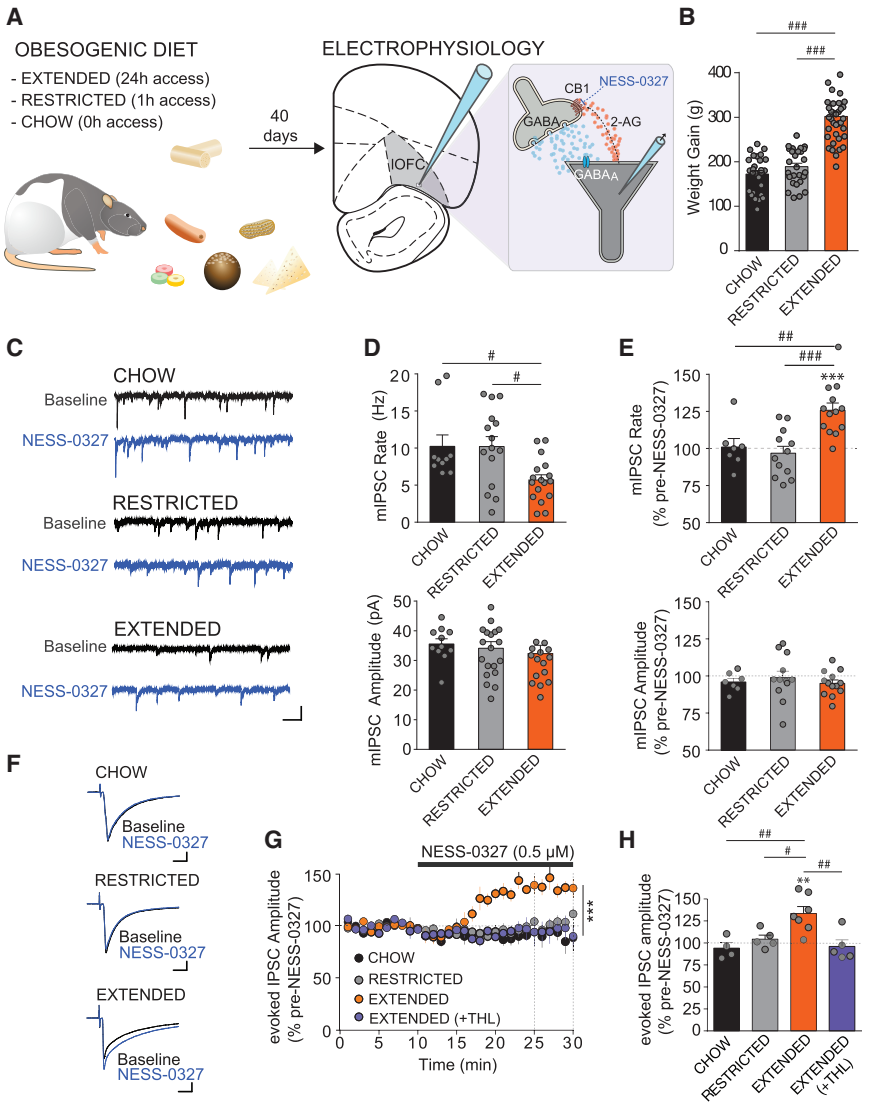

Figure 1. Extended access to a cafeteria diet leads to an endocannabinoid-mediated inhibition of GABAergic synaptic transmission in the OFC

(A) Schematic of experimental paradigm.

(B) Change in body weight following extended (N = 38) or restricted (N = 27) access to a cafeteria diet or chow alone. Extended-access rats gain significantly more weight compared to those with restricted ($p < 0.001$) or chow access ($p < 0.001$). One-way ANOVA, $F[2,89] = 68.49$, $p < 0.001$, Tukey's post hoc tests.

(C) Example traces of mIPSCs before and during application of the neutral CB1R antagonist, NESS-0327 (0.5 μM) in lOFC pyramidal neurons from chow, restricted, or extended-access rats. Scale bars, 50 pA, 100 ms.

(D) Basal rate and amplitude of mIPSCs from chow- (n = 10/6), restricted- (n = 14/7), or extended- (n = 17/8) access rats. Rats given extended access to a cafeteria diet have decreased mIPSC rate compared to chow- and restricted-access rats (one-way ANOVA, $F[2,38] = 5.107$, $p = 0.011$ with Tukey's multiple comparison test). There was no significant difference in mIPSC amplitude between diet groups ($F[2,38] = 0.380$, $p = 0.686$).

(E) NESS-0327 unmasks a facilitation of mIPSC rate in extended-access rats (n = 13/8, $^{###}p < 0.001$), which is significantly different from chow- (n = 8/5, $^{##}p < 0.01$) and restricted- (n = 12/5, $^{###}p < 0.001$) access rats ($F[2,30] = 11.37$, $p = 0.0002$). mIPSC rate in extended-access rats was significantly greater than baseline ($t_{(12)} = 5.326$, $^{***}p = 0.0002$) but not in chow ($t_{(7)} = 0.212$, $p = 0.838$) and restricted-access rats ($t_{(11)} = 0.682$, $p = 0.509$). NESS-0327 had no effect on mIPSC amplitude ($F[2,30] = 0.367$, $p = 0.696$).

(F) Example traces of eIPSC amplitude before and during application of NESS-0327 in chow, restricted, and extended-access rats. Scale bars, 100 pA, 10 ms.

(G) Time course of eIPSC amplitude during application of NESS-0327 in chow- (n = 4/3), restricted- (n = 5/4), and extended- (n = 7/4 without THL, n = 5/4 with THL) access rats. There was a significant interaction of diet group × time ($F[87,527] = 4.960$, $p < 0.0001$) and a main effect of diet ($F[3,19] = 10.89$, $p = 0.002$; RM mixed-effect model [REML]-two-way ANOVA).

(H) NESS-0327 unmasked a facilitation of eIPSC amplitude in extended-access rats ($p < 0.01$), which was blocked in the presence of an inhibitor of 2-AG synthesis, THL ($p > 0.05$) (one-way ANOVA: $F[3,17] = 7.445$, $p = 0.0021$). eIPSC amplitude in extended-access rats (n = 7/4) was significantly greater than pre-NESS-0327 baseline ($t_{(6)} = 4.246$, $^{**}p = 0.0054$), whereas that in chow ($t_{(3)} = 0.9659$, $p = 0.4054$, n = 4/3), restricted access ($t_{(4)} = 0.9428$, $p = 0.3991$, n = 5/4) or extended access+THL ($t_{(4)} = 0.6231$, $p = 0.6231$, n = 5/4) were not.

Bars represent mean ± SEM with individual values overlaid.

RESULTS

An obesogenic diet alters inhibitory GABAergic synaptic transmission via recruitment of endocannabinoids

To determine whether diet-induced obesity alters synaptic function in the lOFC, we gave 24 h (extended), 1 h (restricted), or no access (chow) to a cafeteria diet for 40 consecutive days, including *ad libitum* access to chow (Figure 1A). Consistent with previous reports (Johnson and Kenny, 2010; Rolls et al., 1980; Thompson et al., 2017), rats given extended access to a cafeteria diet gained more weight than those with restricted or chow access (Figure 1B). Weight gain on this diet is associated with a higher energy intake due to consumption of cafeteria diet rather than chow and is associated with elevated plasma leptin and insulin levels consistent with obesity (Thompson et al., 2017). Although restricted-access rats exhibited similar preference and macronutrient intake of cafeteria diet, their weight gain was similar to chow rats (Johnson and Kenny, 2010; Thompson et al., 2017). Thus, restricted-access rats served as a pair-fed control whereby their ability to consume the diet in excess of that eaten by chow controls was prevented by the limited duration of exposure (Ellacott et al., 2010).

To compare GABAergic input to lOFC neurons between the dietary conditions, miniature inhibitory postsynaptic currents

(mIPSCs) were recorded in layer II/III pyramidal neurons from extended-, restricted-, and chow-access rats (Figure 1A). The rate, but not amplitude, of mIPSCs was decreased in extended-access rats compared to chow- or restricted-access rats (Figure 1C,D), consistent with a presynaptic mechanism reported previously (Thompson et al., 2017). To test if these changes were specific to the lOFC, we recorded mIPSCs in the prelimbic cortex and primary motor (M1) cortex, located dorsomedial and dorsal of the lOFC, respectively (Figure S1A). In contrast to the lOFC, mIPSC rate and amplitude were not different between chow- and extended-access rats in the prelimbic or M1 cortex (Figures S1B–S1D).

Obesity is associated with elevated levels of the endocannabinoids (eCBs), 2-arachidonoylglycerol (2-AG), and anandamide (AEA) in the brain and periphery (Gatta-Cherifi and Cota, 2016) and impaired eCB signaling and plasticity (Cristino et al., 2013; Linehan et al., 2018; Massa et al., 2010). We hypothesized that elevated eCBs levels in extended-access rats may suppress mIPSCs in the lOFC. If eCBs are tonically present to suppress GABA release, then blockade of CB1 receptors (CB1Rs) should unmask a facilitation of inhibitory transmission. To test this, we examined the effect of the CB1R antagonist, NESS-0327. We chose a neutral antagonist because this would preclude effects due to constitutive receptor activity, unlike the prototypical CB1R inverse agonist, AM251. Indeed, NESS-0327 facilitated the rate of mIPSCs in extended-access rats (126% ± 5%) but did not change that of restricted- (96% ± 5%), or chow- (101% ± 6%) access rats (Figure 1E). NESS-0327 had no effect on mIPSC amplitude in chow- (96% ± 2%), restricted- (99% ± 5%), or extended- (95% ± 2%) access rats (Figure 1E). Together, this indicates the presence of a basal eCB tone suppressing GABA release onto lOFC neurons from extended but not chow- or restricted-access rats. To confirm that this effect extends to action potential-driven activity, we repeated the experiment with electrically evoked IPSCs (eIPSCs). Similarly, NESS-0327 application unmasked a facilitation of eIPSCs in extended access (133% ± 8%) but not chow- (94% ± 6%) or restricted-access rats (104% ± 5%) (Figures 1F–1H). The facilitation of eIPSC amplitude by NESS-0327 was abolished in slices pre-incubated with the diacylglycerol lipase inhibitor, tetrahydrolipstatin (THL) (96% ± 7%) (Figures 1G and 1H), which prevents the biosynthesis of 2-AG. This indicates the presence of a 2-AG-mediated eCB tone suppressing evoked GABAergic transmission onto lOFC pyramidal neurons in obese rats. To test if eCBs also modulate glutamatergic synapses, we first examined their cannabinoid sensitivity with the CB1R agonist, WIN55,212-2 on evoked excitatory postsynaptic currents (eEPSCs) in chow-access rats. WIN55,212 inhibited eEPSCs in lOFC pyramidal neurons (77% ± 4%) (Figures S2A–S2C). However, NESS-0327 application in extended-access rats did not facilitate eEPSCs (98% ± 6%) (Figures S2D–S2F). Thus, although both excitatory and inhibitory synapses onto lOFC pyramidal neurons are sensitive to eCBs, only inhibitory synapses exhibit an eCB tone during the obese state.

Endocannabinoid-mediated long-term depression is impaired in the OFC of obese rats

We next investigated if eCB tone in the lOFC of obese rats influenced synaptic plasticity. We first tested if inhibitory synapses onto lOFC pyramidal neurons undergo long-term depression (LTD) in diet-naive rats (Figure S3A). Theta-burst stimulation (TBS), mimicking endogenous high-frequency gamma bursts at a lower-frequency theta oscillation (Buzsáki and Wang, 2012), induced a long-lasting suppression of eIPSC amplitude onto lOFC pyramidal neurons (Figures S3B–S3D). This was associated with paired-pulse facilitation (Figure S3E), suggesting a presynaptic mechanism. Furthermore, TBS-LTD was prevented in the presence of the CB1R antagonist, AM251, consistent with eCB-mediated TBS-LTD reported in the visual and somatosensory cortices (Chevaleyre and Castillo, 2004; Jiang et al., 2010; Zhao et al., 2015) (Figures S3B–S3D). Given that many forms of eCB-mediated LTD also depend on activation of group 1 metabotropic glutamate receptors (mGluR1/5), we examined TBS-LTD in the presence of the mGluR5 antagonist, MTEP. Similar to AM251, MTEP abolished LTD and paired-pulse facilitation induced by TBS (Figures S3B–S3E). Thus, TBS can induce LTD of lOFC GABA synapses that is dependent on activation of mGluR5 and eCBs.

We then examined if TBS-LTD was altered by diet-induced obesity. TBS induced a long-term suppression of eIPSCs in lOFC pyramidal neurons from chow- and restricted-access rats (69% ± 9% and 67% ± 5% of baseline, respectively) (Figures 2A and 2B), and this was associated with a paired-pulse facilitation in chow-access rats (Figure 2C). By contrast, TBS had no effect on eIPSCs in extended-access rats (98% ± 4% of baseline) (Figures 2A–2C). Therefore, eCB-mediated LTD is specifically impaired in the lOFC of obese rats.

We next examined whether the obesity-induced eCB tone and impairment of TBS-LTD was mediated upstream by mGluR1/5 activation. Similar to TBS-LTD, the mGluR1/5 agonist, DHPG, produced an LTD of eIPSC amplitude in chow-access rats, which was blocked in the presence of AM251 (Figures 2D and 2E). Consistent with a presynaptic effect, this was associated with paired-pulse facilitation, which was blocked by AM251 (Figure 2F). By contrast, DHPG had no effect on eIPSCs in extended-access rats (Figures 2D–2F). Together, these results indicate that similar to TBS, mGluR1/5 activation induces eCB-mediated LTD. This plasticity is impaired in obese rats, suggesting a disruption in mGluR1/5-eCB signaling.

We subsequently tested if the eCB tone previously revealed by NESS-0327 in obese rats was also mediated by mGluR1/5. In the presence of MTEP, NESS-0327 no longer produced a facilitation of eIPSC amplitude in extended-access rats (Figure 2G), indicating the necessity of mGluR5 activation in mediating eCB tone. Furthermore, MTEP application alone mimicked a facilitation of eIPSCs, similar to NESS-0327 (Figure 2H). Together, these results indicate that mGluR5 activation induces eCB tone, which may occlude the induction of eCB-mediated LTD in the lOFC of obese rats (Figure 2I).

An obesogenic diet induces an extrasynaptic glutamate tone in the OFC

The obesity-induced alteration in mGluR5 signaling may be due to a change in receptor sensitivity, number, or an occlusion by enhanced levels of synaptic glutamate spillover. We first examined basal glutamatergic synaptic input onto lOFC neurons from chow- or extended-access rats (Figure 3A). Although we

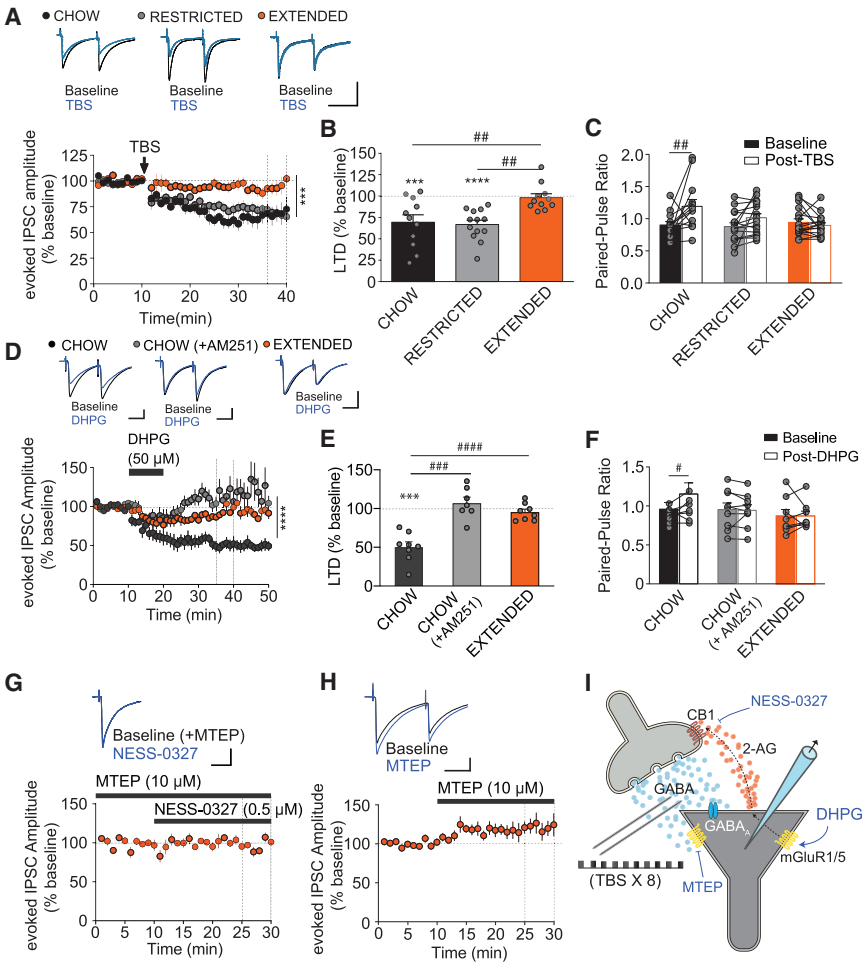

Figure 2. Endocannabinoid-mediated inhibitory LTD is impaired by an obesogenic diet

(A) Time plot of eIPSC amplitude before and after TBS in lOFC neurons from chow- (n = 11/9), restricted- (n = 13/9), or extended- (n = 11/7) access rats. There was a significant interaction of diet group × time ($F[116,2,053] = 2.819$, $p < 0.0001$) and a main effect of diet ($F[2,44] = 11.00$, $^{***}p = 0.0001$; REML two-way ANOVA). Inset: example traces of eIPSC amplitude before and after TBS in chow-, restricted-, or extended-access rats. Scale bars, 200 pA, 20 ms.

(B) TBS-LTD quantified 25–30 min following TBS is inducible in chow- ($^{\#\#}p < 0.01$) and restricted- ($^{\#\#}p < 0.01$) access rats, but is impaired in extended-access rats ($F[2,32] = 7.511$, $p = 0.002$). eIPSC amplitude after TBS is significantly decreased from baseline in chow- ($n = 11/9$, $t_{(10)} = 3.495$, $^{***}p = 0.0058$) and restricted-access rats ($n = 13/9$, $t_{(12)} = 6.637$, $^{****}p < 0.0001$) but not extended- ($n = 11/7$, $t_{(10)} = 0.3991$, $p = 0.6982$) access rats.

(C) A RM two-way ANOVA indicates a significant diet × LTD interaction ($F[2,43] = 5.087$, $p = 0.010$) with a main effect of TBS ($F[1,43] = 8.537$, $p = 0.0055$) the paired-pulse ratio of eIPSCs. A Sidak multiple comparison test reveals a significant effect of TBS on paired-pulse facilitation in chow ($n = 11/9$, $p < 0.01$), but not restricted- ($n = 13/9$) or extended-access rats ($n = 11/7$).

(D) The mGluR1/5 agonist, DHPG induces an LTD in chow- ($n = 10/5$) access rats, which is blocked in slices pre-treated with the CB1R antagonist, AM251 (3 μM, n = 15/5). In contrast, DHPG does not induce LTD in extended- ($n = 12/6$) access rats. REML two-way ANOVA indicates a significant diet group × LTD interaction ($F[78,1,140] = 4.684$, $p < 0.0001$) with a main effect of diet ($F[2,34] = 12.85$, $p < 0.0001$) and a main effect of LTD ($F[5.110,149.4] = 11.59$, $p < 0.0001$). Inset: example traces of eIPSC amplitude before and after application of DHPG (50 μM) in slices from chow, chow+AM251, and extended-access rats. Scale bars, 250 pA, 25 ms.

(E) DHPG produces a long-term suppression of eIPSC amplitude, which is blocked in the presence of AM251 (3 μM) and absent in extended-access rats ($F[2,20] = 23.70$, $p < 0.0001$, Tukey's multiple comparison test: chow ($n = 8/5$) versus chow+AM251 ($n = 7/5$), $^{###}p < 0.001$, chow versus extended ($n = 8/6$), $^{###}p < 0.0001$). eIPSC amplitude after DHPG is significantly decreased from baseline in chow-access rats ($n = 8/5$, $t_{(7)} = 7.37$, $^{***}p = 0.0002$), but not in the presence of AM251 ($n = 7/5$, $t_{(6)} = 0.923$, $p = 0.392$) nor in extended-access rats ($n = 8/6$, $t_{(7)} = 1.18$, $p = 0.276$).

(F) A two-way RM ANOVA: diet × drug interaction ($F[2,23] = 2.690$, $p = 0.089$). A Sidak multiple comparisons test indicates that DHPG elicits paired-pulse facilitation 15–20 min after application in lOFC neurons from chow ($^{\#}p < 0.05$, $n = 9/5$), but not in the presence of AM251 ($n = 9/5$) or in extended-access rats ($n = 8/6$).

(G) The facilitation of eIPSC amplitude by the neutral CB1R antagonist, NESS-0327 is blocked by the mGluR5 antagonist MTEP in lOFC neurons from extended-access rats ($n = 7/5$). Inset: example traces of eIPSC amplitude before and during application of NESS-0327 from slices of extended-access rats pre-incubated with MTEP. Scale bars, 250 pA, 25 ms.

(H) In extended-access rats ($n = 7/5$), MTEP unmasks a facilitation of eIPSC amplitude, indicative of an mGluR5-mediated tone onto lOFC pyramidal neurons. Inset: Example traces of eIPSC amplitude before and during application of MTEP. Scale bars, 250 pA, 25 ms.

(I) Experimental schematic illustrating eCB-mediated inhibitory LTD in OFC pyramidal neurons induced via TBS or group 1 mGluR activation, unmasking of eCB tone via blockade of CB1Rs with NESS-0327.

Bars represent mean ± SEM with individual values overlaid.

observed no change in mEPSC amplitude between diet groups (Figures 3B and 3D), there was a reduction of mEPSC rate in extended compared to chow-access rats (Figures 3B and 3C), indicative of a decrease in presynaptic glutamate release. To further gauge synaptic glutamate levels, we measured effects of the low-affinity α-amino-3-hydroxy-5 -methyl-4-isoxazolepropionic acid receptor (AMPAR) antagonist γ-DGG on AMPAR eEPSCs (Figure 3E). γ-DGG competes with ambient glutamate to bind synaptic AMPARs. Thus, the inhibition of AMPAR eEPSC amplitude produced by γ-DGG inversely correlates with synaptic levels of glutamate. Compared to chow-access rats, γ-DGG produced greater inhibition of AMPAR eEPSCs in extended-access rats (Figures 3F, 3G, and 3I), indicating decreased evoked synaptic glutamate. To determine if this effect was due to a

change in synaptic glutamate or AMPAR number or function, we applied the high-affinity AMPAR antagonist, DNQX, which fully displaces glutamate from synaptic AMPARs. There was no difference in DNQX-induced inhibition of AMPAR eEPSCs in chow- or extended-access rats (Figures 3H and 3I). Contrary to our prediction that synaptic glutamate spillover leads to mGluR5 activation, there is decreased synaptic glutamate release onto lOFC neurons from obese rats.

Given that obese rats have decreased synaptic glutamate release inconsistent with glutamate spillover, we explored an alternate hypothesis that mGluR5s are activated by glutamate from a non-synaptic source. First, to indirectly interrogate levels of extrasynaptic glutamate, we used a high-frequency train of stimulation to evoke glutamate release onto extrasynaptic n-methyl-D-aspartate receptors (NMDARs) (Figures 3J and 3K). Thus, NMDARs served as sensor for extrasynaptic glutamate. To measure the duration of glutamate action at NMDARs, we analyzed the half-decay time of NMDAR eEPSCs. Baseline decay time was prolonged in extended-access rats relative to chow-access rats (Figures 3K and 3L), indicating elevated levels of glutamate in the extrasynaptic space. We then used the glutamate transport inhibitor, DL-TBOA (TBOA) to indirectly assess changes in the efficacy of glutamate transport. In chow-access rats, TBOA produced a 319% ± 37% increase in decay time, but this facilitation was reduced to 164% ± 13% in extended-access rats (Figures 3K and 3M). TBOA was less effective at preventing extrasynaptic glutamate reuptake in extended-access rats, suggesting there is a partial occlusion of NMDARs by extrasynaptic glutamate. Thus, extrasynaptic glutamate tone was likely the result of reduced efficacy of non-synaptic glutamate transporters, rather than synaptic spillover of glutamate.

One possibility for decreased synaptic glutamate release is through autoinhibition via presynaptic mGluR2/3 activation by extrasynaptic glutamate. Therefore, we examined the effect of the mGluR2/3 agonist LY379268 on AMPAR eEPSCs (Figure 4A). LY379268 inhibited eEPSCs from chow-access rats, which was reversed with the mGluR2/3 antagonist, LY341495 (Figures 4B–4D). The LY379268 agonist produced less inhibition of eEPSCs in extended access than chow-access rats (Figures 4B–4D). If an extrasynaptic glutamate tone is suppressing excitatory transmission, an mGluR2/3 antagonist should unmask a facilitation of this response (Figure 4E). The LY341495 antagonist had no effect on eEPSCs in chow-access rats but facilitated this response in extended-access rats (Figures 4F–4H). Together, these data suggest that in obese rats, there is a persistent suppression of synaptic glutamate release via tonic activation of presynaptic mGluR2/3 receptors by extrasynaptic glutamate.

An obesogenic diet induces hypertrophy of astrocytes and impairs their ability to transport glutamate

Given that astrocytes account for the majority of glutamate transport in the brain and are altered in obesity (García-Cáceres et al., 2013), we surmised that an obesogenic diet impairs astrocytes and their ability to uptake glutamate. The intensity and area, but not number of cells expressing the astrocyte marker, of glial fibrillary acidic protein (GFAP) was increased in extended-access rats compared to restricted or chow-access rats (Figures 5A–5F). We next examined OFC astrocytes morphology (Figure 5H) by *in vitro* labeling with the astrocyte-selective dye SR101 and introduction of fluorescein isothiocyanate (FITC)-dextran via patch clamping of individual astrocytes (Figure 5H). In addition to observing typical astrocyte morphology, astrocytes were confirmed electrophysiologically, indicated by a lack of cell firing, low input resistance, and passive membrane conductance (Figure S4). Astrocytes from the lOFC of extended-access rats had larger astrocyte territories (4,407 ± 203 μm^2) compared to those from chow-access rats (3,654 ± 214 μm^2) (Figures 5H–5J) but no change in branching (Figure 5K). Together, these data indicate that extended access to an obesogenic diet induces hypertrophy of OFC astrocytes.

We next explored whether hypertrophic astrocytes in the OFC were associated with impaired glutamate transporter 1 (GLT-1) function, an astrocytic transporter responsible for ~90% of glutamate reuptake in the cortex (Armbruster et al., 2016; Danbolt et al., 1992; Hanson et al., 2016; Voutsinos-Porche et al., 2003). Patch-clamping from SR101-labeled lOFC astrocytes in artificial cerebrospinal fluid (ACSF) containing caged Rubi-Glutamate, we evoked the focal action of glutamate via flash photolysis (Figure 6A). An astrocytic glutamate transporter current was isolated in the presence of synaptic blockers and by subtracting the residual current following application of TBOA (Figure 6B). Glutamate transporter currents in lOFC astrocytes from extended-access rats were reduced compared to those from chow-access rats (Figures 6B and 6C). In contrast to the lOFC, we found that the magnitude of astrocytic GLT-1 currents was not different between chow- and extended-access rats in the prelimbic and motor cortex (Figures S1E and S1F). We further examined GLT-1 protein with western blots but observed no difference in GLT-1 levels between the lOFC of chow- or extended-access rats (Figures 6D and 6E). Together, these results indicate impairment in the function but not quantity of GLT-1 in lOFC astrocytes from obese rats.

We next tested the hypothesis that impairment of astrocytic glutamate transport leads to an eCB-mediated LTD of GABAergic transmission (Figure 6F). Similar to TBS-induced LTD and mGluR-LTD, application of TBOA suppressed eIPSC amplitude in lOFC neurons from chow-access rats, which persisted for at least 20 min after washout of the drug (Figures 6G and 6H). This long-lasting suppression of inhibition was blocked by AM251, indicating that this glutamate transporter-induced effect is eCB-mediated. The TBOA-induced suppression of inhibition was absent in extended-access rats, consistent with an occlusion by extrasynaptic glutamate resulting from impaired transporter function (Figures 6G and 6H). Taken together, these results indicate that inhibition of astrocytic glutamate transport can influence lOFC inhibitory synapses via an eCB-mediated LTD, and this effect is impaired during diet-induced obesity.

Restoration of glutamate homeostasis with N-acetylcysteine reverses the cascade of obesity-induced synaptic deficits

Because altered GABAergic synaptic transmission in lOFC pyramidal neurons from extended-access rats is mediated upstream

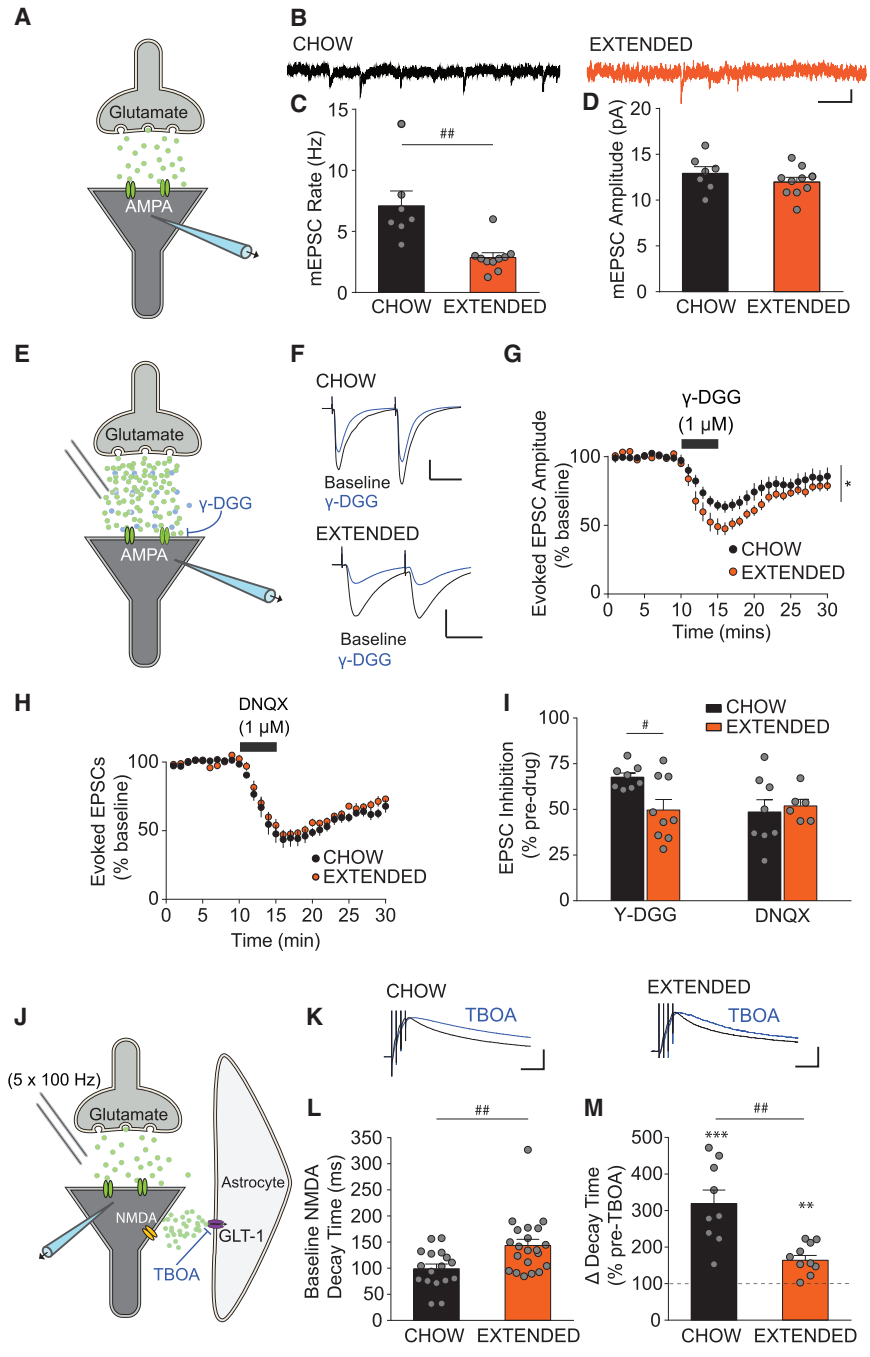

Figure 3. An obesogenic diet alters extrasynaptic and synaptic glutamate via impairment of astrocytic GLT-1

(A) Experimental schematic illustrating recording of mEPSCs in lOFC pyramidal neurons.

(B) Example traces of mEPSCs from chow and extended-access rats. Scale bars, 10pA, 0.1 s.

(C) mEPSC frequency in extended- (n = 10/5) access rats is significantly reduced compared to that of chow- (n = 7/4) access rats ($t_{(15)}$ = 3.82, $^{\#\#}p$ = 0.0017).

(D) mEPSC amplitude is not different between extended- (n = 10/5) and chow- (n = 7/4) access rats ($t_{(15)}$ = 1.11, p = 0.285).

(E) Experimental schematic illustrating the effect of the low-affinity, competitive AMPAR antagonist γ-DGG on AMPAR eEPSCs.

(F) Example traces of AMPAR eEPSCs before and during application of γ-DGG in chow- and extended-access rats (scale bar, 500 pA and 250 pA, 25 ms).

(G) Time plot of AMPAR eEPSC amplitude before and during γ-DGG application in lOFC pyramidal neurons from chow- (n = 8/5) and extended- (n = 9/7) access rats. REML two-way ANOVA reveals a significant diet × time interaction (F[29,422] = 3.135, p < 0.0001), main effect of diet (F[1,15] = 7.683, *p = 0.0142).

(H) Time plot of AMPA eEPSC amplitude before and during application of the high-affinity AMPA receptor antagonist, DNQX in lOFC neurons from chow- (n = 8/5) or extended- (n = 5/4) access rats. REML two-way ANOVA reveals a no diet × time interaction (F[29,290] = 0.531, p = 0.979), or main effect of diet (F[1,11] = 1.130, p = 0.310).

(I) A two-way ANOVA indicates a significant interaction of diet × drug (F[1,26] = 4.45, p = 0.447). A Sidak multiple comparison test indicates that γ-DGG, but not DNQX, alters inhibition of AMPAR eEPSCs in chow compared to extended-access rats ($^{\#}p < 0.05$).

(J) Experimental schematic illustrating the measurement of high-frequency stimulation-induced extracellular glutamate prolonging the decay time of pharmacologically isolated extrasynaptic NMDAR eEPSCs. The effect TBOA (30 μM) was then examined on this measure.

(K) Example traces of NMDAR eEPSCs normalized to peak amplitude before and during application of TBOA (30 μM, 10 mins) in chow- or extended-access rats. Scale bars, 0.5, 50 ms.

(L) Half-decay time of NMDA eEPSCs is significantly longer in extended- (n = 21/5) access rats compared to chow (n = 17/6) rats (unpaired t test, $t_{(36)}$ = 2.89, $^{\#\#}p$ = 0.0065).

(M) Decay time is enhanced by TBOA in both chow- (n = 9/4, $t_{(8)}$ = 5.956, ***p = 0.0003) and extended-access rats (n = 9/6, $t_{(8)}$ = 4.885, **p = 0.0012) compared to baseline. However, this enhancement is significantly reduced in extended-access rats ($t_{(16)}$ = 3.97, $^{\#\#}p$ = 0.0011).

Bars represent mean ± SEM with individual values overlaid.

by impaired glutamate transport, we surmised that restoration of glutamate homeostasis *in vitro* could reverse the cascade of synaptic changes observed with diet-induced obesity. We tested the effect of N-acetylcysteine (NAC), a cystine prodrug reported to enhance GLT-1 activity and restore extrasynaptic glutamate concentration (Kupchik et al., 2012; Reissner et al., 2015). In NAC, GLT-1 currents were enhanced in astrocytes of extended-access rats, restoring their magnitude to that observed in chow-access rats (Figure 7A). This was associated with decreased high-frequency stimulation-evoked NMDAR EPSC decay time and a restoration in the ability of TBOA to enhance this measure (Figure 7B). Taken together, NAC

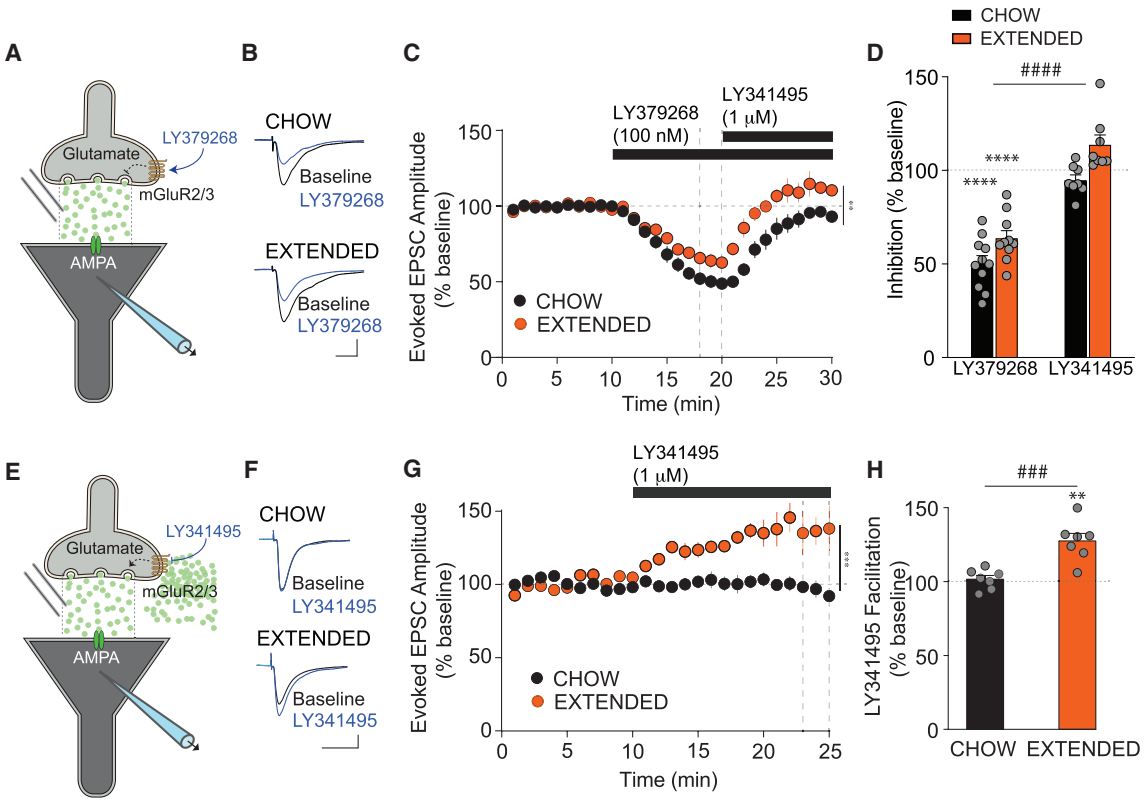

Figure 4. Glutamatergic synapses in obese rats are tonically suppressed by glutamate acting via extrasynaptic mGluR2/3 receptors

(A) Experimental schematic illustrating the effect of the mGluR2/3 agonist LY379268 on AMPA eEPSCs.

(B) Example traces of AMPA eEPSCs before and during application of LY379268 in lOFC neurons from chow- or extended-access rats. Scale bar, 500 pA, 10 ms.

(C) Time plot of eEPSC amplitude before and during application of LY379268 (100 nM) and then after further addition of the mGluR2/3 receptor antagonist, LY341495 in lOFC neurons from chow- (n = 11/4) or extended-access rats (n = 10/4). There was a significant diet × time interaction, $F[29,494] = 4.097$, $p < 0.0001$ and a main effect of diet, $F[1,18] = 11.03$, $^{**}p = 0.0038$.

(D) LY379268 produced significantly more inhibition of eEPSC amplitude in chow- compared to extended-access rats. A REML two-way ANOVA indicated no diet × drug interaction ($F[1,33] = 0.4314$, $p = 0.5159$), but main effects of diet ($F[1,33] = 14.75$, $p = 0.0005^{\#\#\#}$ and drug ($F[1,33] = 125.9$, $^{\#\#\#\#}p < 0.0001$). There was a significant LY379268-induced inhibition of EPSCs compared to baseline in chow- (n = 11/4, $t_{(10)} = 12.06$, $^{****}p < 0.0001$) and extended-access rats (n = 10/4, $t_{(9)} = 8.997$, $^{****}p < 0.0001$).

(E) Experimental schematic illustrating the unmasking of an extrasynaptic glutamate tone suppressing presynaptic glutamate release via blockade of extrasynaptic mGluR2/3 receptors.

(F) Example traces of AMPA eEPSCs before and during application of LY341495 in chow- and extended-access rats. Scale bars, 250 pA, 10 ms.

(G) Time course of eEPSC amplitude before and during application of LY341495 in chow- (n = 7/4) and extended-access rats (n = 7/3). A REML two-way ANOVA indicates a significant diet × time interaction ($F[24,296] = 12.40$, $p < 0.0001$) and a significant diet effect: ($F[1,13] = 24.35$, $^{***}p = 0.0003$).

(H) There was a significant difference in eEPSC facilitation by LY341495 between chow- (n = 7/4) and extended-access rats ($t_{(12)} = 4.57$, $^{\#\#\#}p = 0.0006$, n = 7/3). There was a significant LY341495-induced facilitation of EPSCs over baseline in extended-access rats ($t_{(6)} = 5.424$, $^{**}p = 0.0016$), but not chow-access rats ($t_{(6)} = 0.6378$, $p = 0.5471$).

Bars represent mean ± SEM with individual values overlaid.

enhances the function of astrocytic glutamate transporters, leading to decreased extrasynaptic glutamate onto lOFC pyramidal neurons of obese rats.

We then tested whether NAC could abolish the mGluR5-induced eCB tone and restore LTD at inhibitory synapses. Pre-treatment with NAC prevented the facilitation of eIPSC amplitude induced by NESS-0327 (Figures 7C and 7D) and restored both mGluR-LTD and TBS-LTD at inhibitory synapses onto lOFC neurons (Figures 7E–7G). To confirm that NAC restores eCB tone and TBS-LTD through manipulation of glutamate transport, we re-examined the effect of NAC with the selective GLT-1 blocker dihydrokainic acid (DHK). DHK prevented the NAC restoration of eCB tone (Figures 7C and 7D) and blocked TBS-induced LTD (Figures 7F and 7G), indicating that NAC rescues these synaptic changes by restoring astrocyte glutamate clearance. Finally, NAC pre-treatment enhanced mIPSCs frequency in extended-access rats, similar to that of chow-access rats (Figure 7H). However, NAC did not alter mIPSC frequency in chow-access rats, suggesting an action specific to the obese state. Additionally, application of the GLT-1 inhibitor prevented the NAC-induced restoration of mIPSC frequency (Figure 7H), further confirming a mechanism of action via GLT-1. Together, these data indicate that by restoring glutamate transporter function and extrasynaptic glutamate levels, NAC abolishes eCB

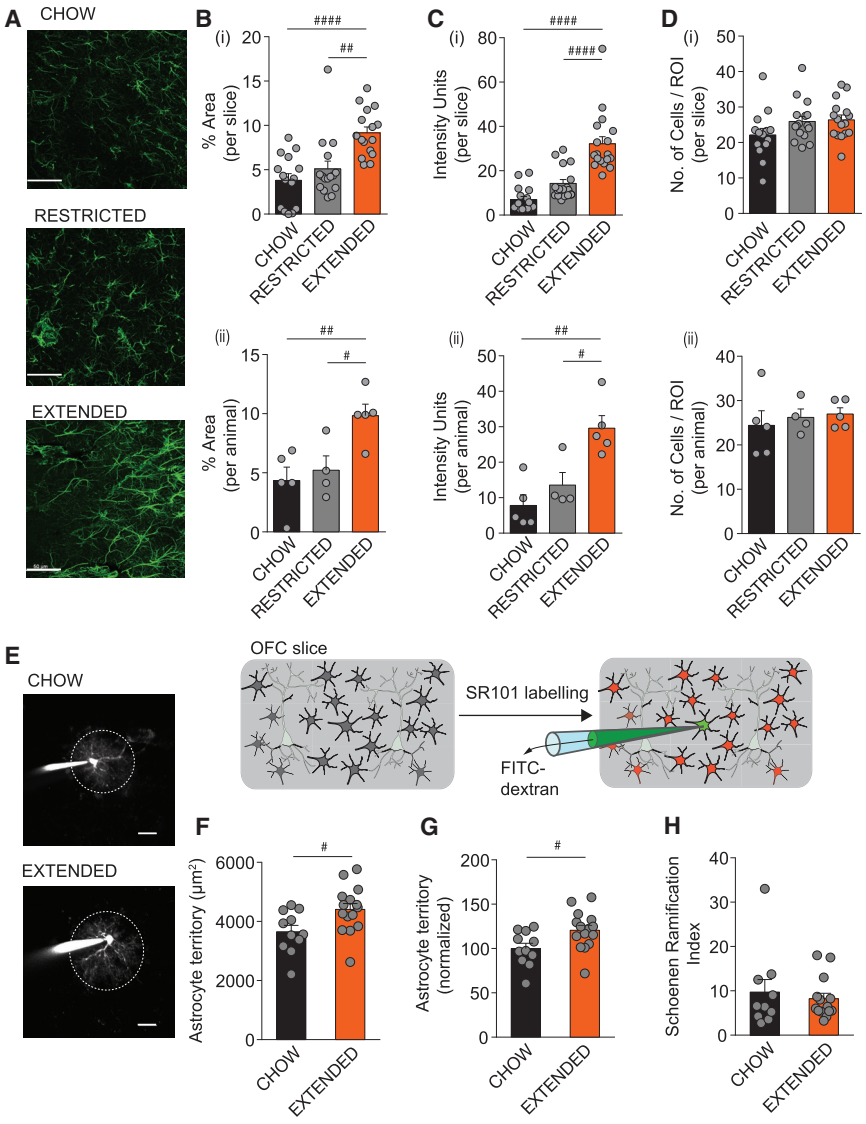

Figure 5. OFC astrocytes are hypertrophic following extended exposure to an obesogenic diet

(A) Representative images illustrating GFAP immunofluorescence in the lOFC of chow-, restricted-, and extended-access rats. Scale bar, 50 µm.

(B) Percentage area of GFAP staining in lOFC shown (1) individually per slice or (2) averaged per animal. GFAP area in extended-access rats (n/N = 14/5) is greater than that from chow (n/N = 12/5; $^{####}p < 0.0001$ individual; $^{##}p < 0.01$ averaged) or restricted- (n/N = 16/4; $^{##}p < 0.01$ individual; $^{#}p < 0.05$ averaged) access rats. One-way ANOVA: F [2,44] = 13.29, p < 0.0001, individual; F[2,11] = 7.526, p = 0.0087, averaged.

(C) Intensity of GFAP staining in lOFC shown (1) individually per slice or (2) averaged per animal. GFAP intensity is greater in extended-access rats (n/N = 18/5) compared to that from chow- (n/N = 16/5; $^{####}p < 0.0001$ individual; $^{##}p < 0.01$ averaged) or restricted- (n/N = 17/4; $^{###}p < 0.0001$ individual; $^{#}p < 0.05$ averaged) access rats. One-way ANOVA: F[2,48] = 31.85, p < 0.0001, individual); one-way ANOVA: F[2,11] = 12.08, p = 0.0017, averaged).

(D) Quantity of GFAP^{+} cells in the lOFC of extended- (n/N = 14/5), restricted- (n/N = 16/4), or chow- (n/N = 12/5) access rats shown (1) individually per slice or (2) averaged per animal. There is no significant difference in the number of GFAP^{+} cells between groups. One-way ANOVA: F[2,43] = 2.207, p = 0.1223, individual; one-way ANOVA: F [2,11] = 0.314, p = 0.737, averaged.

(E) Representative images illustrating fluorescent dye-filling of astrocytes within layer II/III of the lOFC in slices from chow- and extended-access rats. Scale bars, 10 µm. Inset: experimental schematic outlining imaging of astrocyte processes.

(F) Astrocyte territory is significantly increased in lOFC from extended-access rats (n = 15/4) compared to chow-access rats (n = 11/4) ($t_{(24)}$ = 2.514, $^{#}p = 0.019$).

(G) Normalized astrocyte territory is significantly increased in lOFC from extended-access rats (n = 15/4) compared to chow-access rats (n = 11/4) ($t_{(24)}$ = 2.514, $^{#}p = 0.019$).

(H) Astrocyte Schoenen ramification index is not different between chow- (n = 10/4) and extended- (n = 14/4) access rats ($t_{(22)}$ = 0.532, p = 0.6003).

Bars represent mean ± SEM with individual values overlaid.

tone and the occlusion of eCB-mediated LTD, thereby rescuing the impairment of GABAergic synaptic transmission in obese rats.

DISCUSSION

This study provides a number of insights that expand our understanding of how obesogenic diets alter synaptic function in the brain. Our data identify a series of alterations in astrocytes and neurons that become disrupted in obesity. Following long-term exposure to an obesogenic diet, lOFC astrocytes undergo hypertrophy and impairment of GLT-1. This leads to enhanced extrasynaptic glutamate, which generates an eCB tone via mGluR5 activation to induce an LTD of GABA transmission onto lOFC pyramidal neurons. Importantly, this cascade of synaptic deficits could be reversed by restoring astrocyte regulation of glutamate homeostasis with the nutritional supplement, NAC. Thus, an obesogenic diet acts via an astrocyte-neuron interaction to induce heterosynaptic plasticity of excitatory and inhibitory synapses within the lOFC.

An obesogenic diet alters astrocyte structure and function in the OFC

Extended access to an obesogenic diet led to hypertrophy of OFC astrocytes, whereby their territorial domain expanded by ~20%. This was accompanied by increased GFAP immunoreactivity, which may be indicative of reactive astrocytes, although not an absolute marker (Escartin et al., 2021). This is consistent with astrocyte reactivity reported in the hypothalamus following short- or long-term obesogenic diet exposure (Thaler et al.,

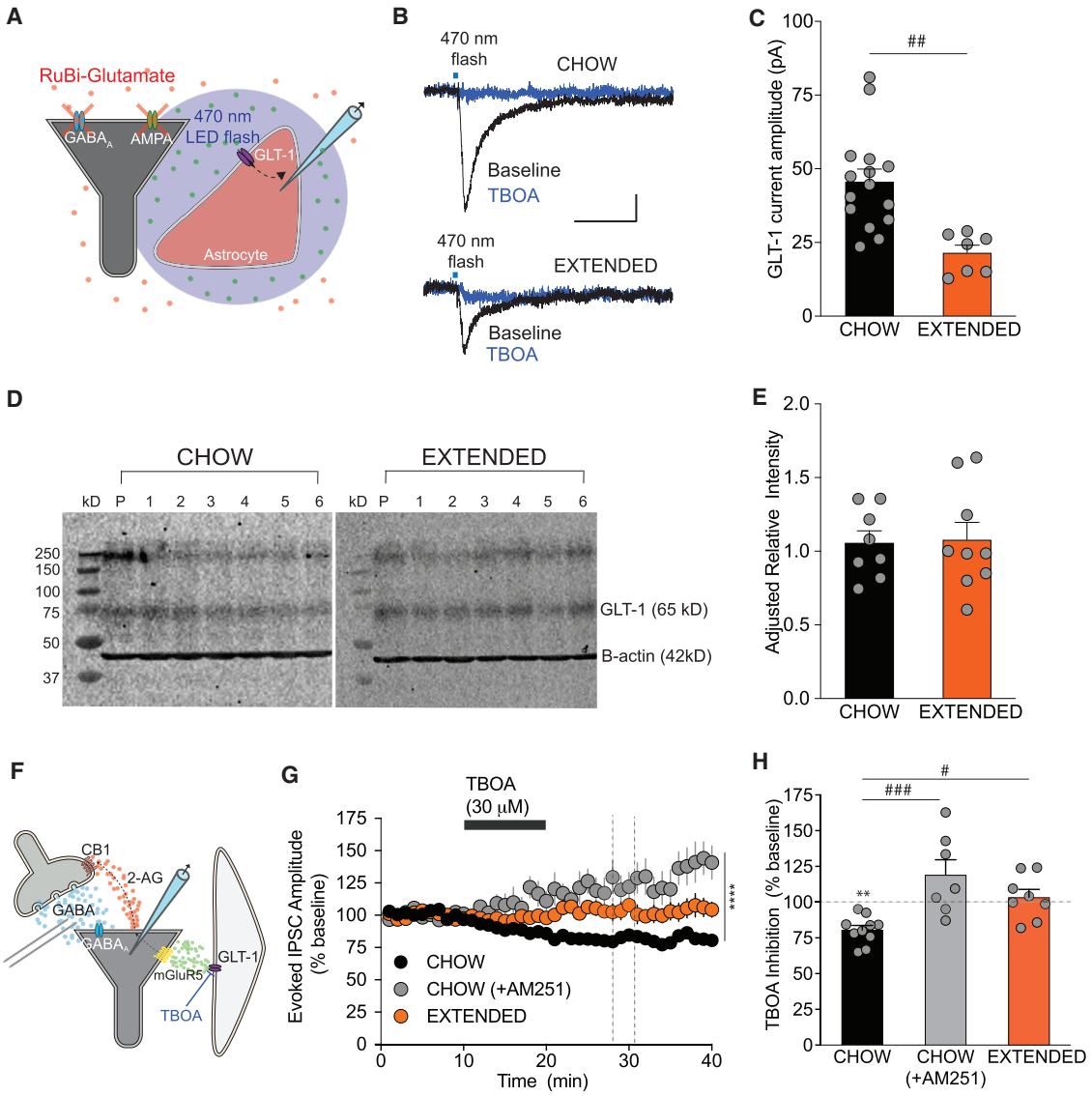

Figure 6. OFC astrocytes have impaired glutamate transport following extended exposure to an obesogenic diet

(A) Experimental schematic illustrating the recording of glutamate transporter currents in astrocytes evoked via flash photolysis of caged RuBi-Glutamate before and during application of the glutamate transport blocker TBOA (30 μM).

(B) Example traces of astrocyte glutamate transporter currents in the lOFC of chow- and extended-access rats. Scale bar, 10 pA, 25 ms.

(C) GLT-1 current amplitude is significantly reduced in lOFC astrocytes from extended- (n = 7/4) compared to chow- (n = 15/5) access rats ($t_{(20)} = 3.664$, $^{\#\#}p = 0.0015$).

(D) Example immunoblots of GLT-1 (65 kDa) and beta-actin (42 kDa) from the OFC of chow- or extended-access rats. Lane numbers refer to OFC samples from different chow- or extended-access rats or the pooled control (P) containing mixed cortex, hippocampus, and striatum.

(E) There is no difference in GLT-1 protein in the OFC of chow- (N = 8) or extended- (N = 9) access rats ($t_{(15)} = 0.159$, $p = 0.88$).

(F) Experimental schematic illustrating a glutamate transporter-induced inhibitory LTD.

(G) TBOA induces an LTD of eIPSCs in lOFC pyramidal neurons from chow-access rats (n = 10/8). This effect is inhibited when slices are pre-treated with AM251 (3 μM, n = 7/5). TBOA-induced LTD is occluded in extended-access rats (n = 8/3). REML two-way ANOVA: $F[1.226,63.14] = 102.9$, $p < 0.0001$.

(H) TBOA-induced inhibition of eIPSC amplitude in chow-access rats (n = 10/8) is blocked in the presence of AM251 (n = 7/5) and absent in extended-access rats (n/N = 8/3). One-way ANOVA: $F[2,22] = 9.804$, $p = 0.0009$, Tukey's multiple comparison test: chow versus chow+AM251, $^{\#\#\#}p < 0.001$, chow versus extended, $^{\#}p < 0.05$. Compared to baseline, TBOA significantly decreased eIPSC amplitude in chow-access rats ($t_{(9)} = 6.307$, $^{***}p = 0.0001$) but not lOFC neurons of chow-access animals pre-treated with AM251 ($t_{(6)} = 1.824$, $p = 0.1180$) or from extended-access rats ($t_{(7)} = 0.6321$, $p = 0.5474$).

Bars represent mean ± SEM with individual values overlaid.

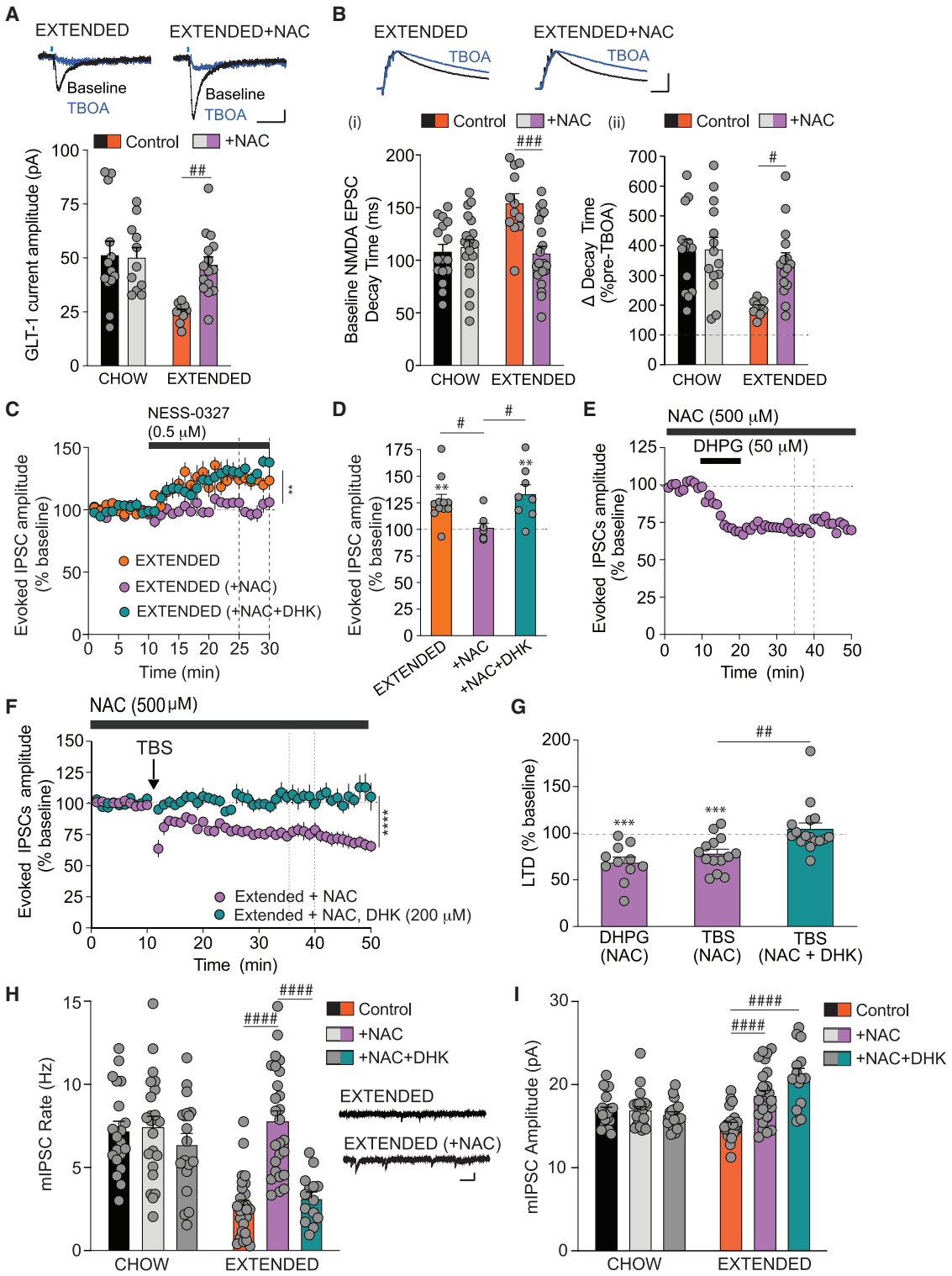

Figure 7. Restoration of glutamate homeostasis via astrocytic GLT-1 reverses the cascade of diet-induced alterations impairing inhibitory synaptic plasticity

(A) NAC enhances GLT-1 currents in astrocytes from extended-access rats (chow: n = 13/4; chow+NAC: n = 11/4; extended: n = 10/5; extended+NAC: n = 15/5). There was a significant diet × drug interaction ($F[1,45] = 5.847$, $p = 0.197$) with main effects of diet ($F[1,45] = 4.698$, $p = 0.0355$) and drug ($F[1,45] = 9.675$, $p =$

(legend continued on next page)

2012; Zhang et al., 2017). Given that the ability of astrocytes to modify synaptic function relies on their physical interaction with synapses (Pannasch et al., 2014; Papouin et al., 2017), alterations in astrocyte territory are likely to impact basal synaptic activity. Indeed, astrocytes can directly influence glutamate transport by expanding or retracting their GLT-1 containing processes in an activity-dependent manner. (Oliet et al., 2001; Pannasch et al., 2014). Furthermore, GLT-1 can mobilize in the membrane to influence glutamate kinetics (Murphy-Royal et al., 2015). Consistent with this, we observed altered kinetics of extrasynaptic glutamate action induced by obesity. Although this was linked to impaired clearance via reduced GLT-1 function, we additionally observed an expansion of OFC astrocyte processes without a change in GLT-1 quantity, suggesting that the density of GLT-1 may be reduced during obesity. Thus, it is conceivable that a diluted presence of astrocytic GLT-1 may negatively impact glutamate homeostasis by disconnecting glutamate reuptake from synaptic release. Other studies using obesogenic diets have reported mixed findings in GLT-1 number, demonstrating both a reduction (Linehan et al., 2018; Tsai et al., 2018) or increase in hypothalamic or hippocampal tissue (Cano et al., 2014; Valladolid-Acebes et al., 2012). These discrepant findings may perhaps be explained by differing changes in astrocyte morphology, depending on type and duration of diet (Zhang et al., 2017).

A consequence of reduced astrocytic glutamate transport in the OFC of obese rats was a tonic presence of glutamate in the extrasynaptic space. This excess of extrasynaptic glutamate indirectly led to downstream suppression of synaptic GABA (via mGluR5-induced eCB signaling) and glutamate (via mGluR2/3-mediated autoinhibition). Thus, by altering extrasynaptic glutamate transport, an obesogenic diet engages distinct mGluR mechanisms to modulate inhibitory and excitatory synaptic transmission.

An obesogenic diet disrupts eCB-mediated inhibitory synaptic plasticity in the OFC

Rats with extended access to a cafeteria diet exhibited decreased GABA release onto layer II/III pyramidal neurons within the lOFC, consistent with our previous findings (Thompson et al., 2017). This was accompanied by elevated eCB tone. These obesity-induced synaptic changes were associated with an inability to induce eCB-mediated LTD, indicating that eCBs induce a prior experience of plasticity resulting in a persistent suppression of inhibition. As a result of impaired astrocytic GLT-1 function, leading to increased extrasynaptic glutamate, we showed that this eCB tone was mediated via activation of Group 1 mGluRs. Together, our results identify a complex mechanism by which a failure in glutamate reuptake by astrocytes can heterosynaptically modulate GABAergic transmission via

0.0032). A Sidak multiple comparison's test revealed a significant difference between control and NAC in the extended access group ($^{\#\#}p = 0.0044$). Inset: example traces of GLT-1 currents in untreated and NAC-treated lOFC slices from extended-access rats. Scale bars, 10 pA, 25 ms.

(B) (1) NAC reduces baseline NMDA eEPSC half-decay time in lOFC pyramidal neurons from extended, but not chow-access rats (chow: n = 16/6; chow+NAC: n = 20/6; extended: n = 12/4; extended+NAC: n = 22/7; interaction: $F[1,66] = 11.66$, $p = 0.0011$; diet effect: $F[1,66] = 6.851$, $p = 0.0110$; drug effect: $F[1,66] = 0.8,043$, $p = 0.0061$). A Sidak post hoc test indicated a significant difference between control and NAC in the extended access group ($^{\#\#\#}p < 0.001$). (2) There was a significant interaction of diet and NAC on the change in decay time by TBOA ($F[1,47] = 4.055$, $p = 0.49$) and a main effect of diet ($F[1,47] = 10.01$, $p = 0026$) and a main effect of NAC ($F[1,47] = 4.811$, $p = 0.033$). A Sidak post hoc test reveals a significant difference between control (n = 9/3) and NAC (n = 15/6) in the extended access group ($^{\#}p = 0.0129$), but not chow NAC treated (n = 13/4) or untreated (n = 13/4) neurons. Inset: example traces of NMDAR eEPSCs normalized to peak from lOFC pyramidal neurons from untreated and NAC-treated slices from extended-access rats. Scale bars, 0.5, 50 ms.

(C) NAC treatment (n = 8/6) abolishes the facilitation of eIPSC amplitude unmasked by NESS-0327 in lOFC neurons from extended-access rats (n = 11/9). This effect is reversed by the selective GLT-1 blocker, DHK (200 μM, n = 8/6). A REML two-way ANOVA indicates a significant NAC treatment × time interaction ($F[58,686] = 2.441$, $^{\#\#\#\#}p < 0.0001$) and a main effect of drug treatment ($F[2,24] = 6.593$, $^{\#\#}p < 0.001$).

(D) There was a significant increase of eIPSC amplitude over baseline with NESS-0327 treatment in extended-access rats (n = 11/9; $t_{(10)} = 4.235$, $^{**}p = 0.0017$), but not in NAC (n = 8/6, $t_{(7)} = 0.338$, $p = 0.745$). The effect of NAC was prevented by DHK (n = 8/6, $t_{(7)} = 3.755$, $^{**}p = 0.0071$). A one-way ANOVA indicates a significant group difference ($F[2,24] = 5.646$, $p = 0.0098$) and a Tukey's post hoc test indicates significant differences between control and NAC ($^{\#}p < 0.05$), and NAC and NAC+DHK ($^{\#}p < 0.05$).

(E) NAC treatment restores the ability to induce DHPG-induced LTD in lOFC neurons from extended-access rats pre-treated with NAC (n = 11/8).

(F) TBS-LTD was restored in extended-access rats pre-treated with NAC (n = 14/7) but not in the additional presence of DHK (n = 16/12) (REML two-way ANOVA: time × drug interaction: $F[48,1,270] = 5.302$, $p < 0.0001$; drug effect: $F[1,28] = 20.96$, $^{****}p < 0.0001$).

(G) NAC treatment restores the ability to induce TBS-LTD (n = 14/7) ($t_{(13)} = 4.564$, $^{***}p = 0.0005$, one-sample t test difference from baseline) or mGluR-LTD (n = 16/12) ($t_{(10)} = 5.303$, $^{***}p = 0.0003$, one-sample t test difference from baseline) in lOFC neurons from extended-access rats. The rescue of TBS-LTD was prevented in the presence of DHK ($t_{(15)} = 0.673$, $p = 0.5024$, one-sample t test compared to baseline). There was a significant difference between groups (one-way ANOVA $F[2,38] = 9.992$, $p = 0.003$, Tukey's post hoc test: NAC-TBS versus NAC-TBS+DHK, $^{\#\#}p < 0.01$).

(H) Effect of NAC on mIPSC rate in lOFC pyramidal neurons from chow- or extended-access rats (two-way ANOVA, diet × drug interaction: $F[2,122] = 10.65$, $p < 0.0001$; diet effect: $F[1,122] = 26.88$, $p < 0.0001$; drug effect: $F[2,122] = 16.03$, $p < 0.0001$). A Tukey's post hoc test indicates that NAC treatment enhances mIPSC rate in lOFC neurons from extended-access rats (extended [n = 26/3] versus extended+NAC [n = 26/3], $^{\#\#\#\#}p < 0.0001$), but had no effect in chow-access rats (chow [n = 20/3] versus chow+NAC [n = 24/3], $p > 0.05$). Further, mIPSC rate was significantly different between lOFC neurons of chow- and extended-access rats ($^{\#\#\#\#}p < 0.0001$). Controls were not significantly different from NAC+DHK treatment in either chow- (n = 16/3; $p > 0.05$) or extended-access rats (n = 14/3; $p > 0.05$). Inset: example traces of mIPSCs in untreated and NAC-treated slices from extended-access rats. Scale bar, 20 pA, 100 ms.

(I) Effect of NAC on mIPSC amplitude in lOFC pyramidal neurons from chow- or extended-access rats (two-way ANOVA: diet × drug interaction: $F[2,122] = 16.22$, $p < 0.0001$; diet effect: $F[1,122 = 12.26]$, $p = 0.0006$; drug effect: $F[2,122] = 12.51$, $p < 0.0001$). A Tukey's post hoc test indicates that NAC increased mIPSC amplitude in extended- ($^{\#\#\#\#}p < 0.0001$) but not chow-access rats ($p > 0.05$). There was no significant difference between chow control and NAC+DHK treatment ($p > 0.05$). In extended-access rats, NAC+DHK treatment significantly increased mIPSC amplitude compared to controls ($^{\#\#\#\#}p < 0.0001$) but was not significantly different from NAC treated ($p > 0.05$).

Bars represent mean ± SEM with individual values overlaid.

recruitment of eCBs. Although manipulation of synaptic glutamate spillover can induce eCB-mediated suppression of GABAergic synapses in neurons under physiological conditions (Chevaleyre and Castillo, 2004; Drew et al., 2008), we demonstrate that astrocyte dysfunction can drive this phenomenon during obesity.

There are multiple consequences of elevated eCB tone in the OFC of obese mice. Dendritic spine density is reduced following chronic cannabinoid exposure (Chen et al., 2013; Rubino et al., 2009). We previously observed a reduction of spine density on lOFC pyramidal neurons in rats exposed to a cafeteria diet (Thompson et al., 2017). Thus, the persistent eCB tone induced by obesity may influence structural plasticity of lOFC pyramidal neurons. Alterations in the eCB system also disrupt the interplay of synaptic excitation and inhibition influencing cortical processing. Notably, deletion of CB1Rs from OFC output neurons disrupts eCB regulation of terminals in the dorsal striatum, leading to habit formation (Gremel et al., 2016). Further, activation of CB1Rs in the OFC influences cost-benefit decision making (Khani et al., 2015). Thus, disrupted eCB regulation of OFC principal output neurons may be implicated in driving inflexible behavior.

The obesity-induced synaptic alterations observed here are not ubiquitous in the frontal cortex. In addition to the OFC, we examined upstream GLT-1 function and downstream GABA transmission in two adjacent regions in the coronal plane, the primary motor cortex and prelimbic cortex. By contrast, both these measures were unaltered by diet, suggesting specificity to the OFC. However, we cannot rule out similar changes in other regions of the cortex or brain.

NAC restores the obesity-induced alterations in excitatory and inhibitory plasticity

There is an increasing body of work indicating that NAC has efficacy in the treatment of neuropsychiatric conditions, including substance use disorder and compulsive behaviors (Baker et al., 2003; Brown et al., 2013; Grant et al., 2009, 2016; Moussawi et al., 2009). NAC appears to restore aberrant glutamate homeostasis by enhancing both cystine-glutamate exchange and glutamate transport via GLT-1 (Kupchik et al., 2012; Reissner et al., 2015). Although existing work supports a therapeutic potential of NAC in treating obesity through its traditional anti-inflammatory and antioxidant properties of restoring glutathione levels, and its ability to interfere with adipogenesis (Dludla et al., 2019), its role in restoring obesity-related glutamatergic alterations in the brain has yet to be demonstrated. Here, we showed that by enhancing GLT-1 activity, NAC reverses the cascade of obesity-induced synaptic changes in the OFC. However, we cannot rule out an antioxidant action via glutathione restoration, given that GLT-1 function may be impaired under conditions of oxidative stress (Lauderback et al., 2001). Taken together, our data indicates that NAC can reverse the cellular alterations induced by an obesogenic diet in the OFC, suggesting a therapeutic potential in ameliorating the functional deficits associated with obesity. Although prior human and animal work has demonstrated efficacy of NAC in reducing food-intake and weight gain (Dludla et al., 2019; Hurley et al., 2016), whether NAC elicits these effects via action within the OFC remains to be determined. Our findings have identified an extended cellular mechanism of action by NAC, which in addition to restoring glutamate homeostasis, may also normalize GABA levels within the brain.

In conclusion, our findings provide a cellular mechanism by which an obesogenic diet links to synaptic alterations within the OFC. By inducing structural and functional plasticity in astrocytes, an obesogenic diet disrupts glutamate homeostasis, leading to a persistent suppression of GABA transmission via recruitment of the eCB system. Together, disinhibition of the OFC may ultimately disrupt the excitatory-inhibitory balance and pyramidal neuron output from this region, which could underlie maladaptive behaviors associated with overeating, leading to a persistence of obesity.

STAR★METHODS

Detailed methods are provided in the online version of this paper and include the following:

- KEY RESOURCES TABLE
- RESOURCE AVAILABILITY
  - Lead contact
  - Materials availability
  - Data and code availability
- EXPERIMENTAL MODEL AND SUBJECT DETAILS
- METHOD DETAILS
  - Location
  - Diets
  - Slice preparation
  - Neuronal Electrophysiology
  - Astrocyte electrophysiology
  - Astrocyte Dye-filling
  - Western Blot Analysis
  - Immunohistochemistry
- QUANTIFICATION AND STATISTICAL ANALYSIS

SUPPLEMENTAL INFORMATION

Supplemental information can be found online at https://doi.org/10.1016/j.celrep.2021.109563.

ACKNOWLEDGMENTS

We acknowledge the Hotchkiss Brain Institute optogenetic core facility and the advanced microscopy facility for their technical support. We also thank Churmy Fan for contributing an illustration. This research was supported by a Koopmans Research Award, Canadian Institutes of Health Research operating grant (FDN-147473), and a Canada Research Chair Tier 1 (950-232211) to S.L.B. B.K.L. was supported by postdoctoral awards from the Cumming School of Medicine (Eyes High) and Alberta Innovates Health Solutions.

AUTHOR CONTRIBUTIONS

B.K.L. designed, performed, and analyzed all electrophysiological experiments with supervision of S.L.B. C.M.-R. performed astrocyte-labeling experiments with supervision of G.R.G. and J.S.B. M.K. and M.Q. performed immunohistochemistry experiments and western blots under the supervision of S.L.B. B.K.L. and S.L.B. wrote the manuscript.

DECLARATION OF INTERESTS

The authors declare no competing interests.

Received: July 1, 2020
Revised: May 3, 2021
Accepted: July 28, 2021
Published: August 17, 2021

REFERENCES

Armbruster, M., Hanson, E., and Dulla, C.G. (2016). Glutamate Clearance Is Locally Modulated by Presynaptic Neuronal Activity in the Cerebral Cortex. J. Neurosci. *36*, 10404–10415.

Baker, D.A., McFarland, K., Lake, R.W., Shen, H., Tang, X.-C., Toda, S., and Kalivas, P.W. (2003). Neuroadaptations in cystine-glutamate exchange underlie cocaine relapse. Nat. Neurosci. *6*, 743–749.

Brown, R.M., Kupchik, Y.M., and Kalivas, P.W. (2013). The story of glutamate in drug addiction and of N-acetylcysteine as a potential pharmacotherapy. JAMA Psychiatry *70*, 895–897.

Buzsáki, G., and Wang, X.-J. (2012). Mechanisms of gamma oscillations. Annu. Rev. Neurosci. *35*, 203–225.

Cano, V., Valladolid-Acebes, I., Hernández-Nuño, F., Merino, B., Del Olmo, N., Chowen, J.A., and Ruiz-Gayo, M. (2014). Morphological changes in glial fibrillary acidic protein immunopositive astrocytes in the hippocampus of dietary-induced obese mice. Neuroreport *25*, 819–822.

Chen, R., Zhang, J., Fan, N., Teng, Z.-Q., Wu, Y., Yang, H., Tang, Y.-P., Sun, H., Song, Y., and Chen, C. (2013). Δ9-THC-caused synaptic and memory impairments are mediated through COX-2 signaling. Cell *155*, 1154–1165.

Chen, C., Jiang, Z., Fu, X., Yu, D., Huang, H., and Tasker, J.G. (2019). Astrocytes Amplify Neuronal Dendritic Volume Transmission Stimulated by Norepinephrine. Cell Rep. *29*, 4349–4361.e4.

Chevaleyre, V., and Castillo, P.E. (2004). Endocannabinoid-mediated metaplasticity in the hippocampus. Neuron *43*, 871–881.

Cristino, L., Busetto, G., Imperatore, R., Ferrandino, I., Palomba, L., Silvestri, C., Petrosino, S., Orlando, P., Bentivoglio, M., Mackie, K., and Di Marzo, V. (2013). Obesity-driven synaptic remodeling affects endocannabinoid control of orexinergic neurons. Proc. Natl. Acad. Sci. USA *110*, E2229–E2238.

Danbolt, N.C., Storm-Mathisen, J., and Kanner, B.I. (1992). An [Na+ + K+] coupled L-glutamate transporter purified from rat brain is located in glial cell processes. Neuroscience *51*, 295–310.

Dludla, P.V., Mazibuko-Mbeje, S.E., Nyambuya, T.M., Mxinwa, V., Tiano, L., Marcheggiani, F., Cirilli, I., Louw, J., and Nkambule, B.B. (2019). The beneficial effects of N-acetyl cysteine (NAC) against obesity associated complications: A systematic review of pre-clinical studies. Pharmacol. Res. *146*, 104332.

Douglass, J.D., Dorfman, M.D., and Thaler, J.P. (2017). Glia: silent partners in energy homeostasis and obesity pathogenesis. Diabetologia *60*, 226–236.

Drew, G.M., Mitchell, V.A., and Vaughan, C.W. (2008). Glutamate spillover modulates GABAergic synaptic transmission in the rat midbrain periaqueductal grey via metabotropic glutamate receptors and endocannabinoid signaling. J. Neurosci. *28*, 808–815.

Ellacott, K.L.J., Morton, G.J., Woods, S.C., Tso, P., and Schwartz, M.W. (2010). Assessment of feeding behavior in laboratory mice. Cell Metab. *12*, 10–17.

Escartin, C., Galea, E., Lakatos, A., O'Callaghan, J.P., Petzold, G.C., Serrano-Pozo, A., Steinhäuser, C., Volterra, A., Carmignoto, G., Agarwal, A., et al. (2021). Reactive astrocyte nomenclature, definitions, and future directions. Nat. Neurosci. *24*, 312–325.

García-Cáceres, C., Yi, C.-X., and Tschöp, M.H. (2013). Hypothalamic astrocytes in obesity. Endocrinol. Metab. Clin. North Am. *42*, 57–66.

Gatta-Cherifi, B., and Cota, D. (2016). New insights on the role of the endocannabinoid system in the regulation of energy balance. Int. J. Obes. *40*, 210–219.

Grant, J.E., Odlaug, B.L., and Kim, S.W. (2009). N-acetylcysteine, a glutamate modulator, in the treatment of trichotillomania: a double-blind, placebo-controlled study. Arch. Gen. Psychiatry *66*, 756–763.

Grant, J.E., Chamberlain, S.R., Redden, S.A., Leppink, E.W., Odlaug, B.L., and Kim, S.W. (2016). N-Acetylcysteine in the Treatment of Excoriation Disorder: A Randomized Clinical Trial. JAMA Psychiatry *73*, 490–496.

Gremel, C.M., Chancey, J.H., Atwood, B.K., Luo, G., Neve, R., Ramakrishnan, C., Deisseroth, K., Lovinger, D.M., and Costa, R.M. (2016). Endocannabinoid Modulation of Orbitostriatal Circuits Gates Habit Formation. Neuron *90*, 1312–1324.

Hall, K.D., and Guo, J. (2017). Obesity Energetics: Body Weight Regulation and the Effects of Diet Composition. Gastroenterology *152*, 1718–1727.e3.

Hanson, E., Danbolt, N.C., and Dulla, C.G. (2016). Astrocyte membrane properties are altered in a rat model of developmental cortical malformation but single-cell astrocytic glutamate uptake is robust. Neurobiol. Dis. *89*, 157–168.

Hirase, H., Iwai, Y., Takata, N., Shinohara, Y., and Mishima, T. (2014). Volume transmission signalling via astrocytes. Philos. Trans. R. Soc. Lond. B Biol. Sci. *369*, 20130604.

Hurley, M.M., Resch, J.M., Maunze, B., Frenkel, M.M., Baker, D.A., and Choi, S. (2016). N-acetylcysteine decreases binge eating in a rodent model. Int. J. Obes. *40*, 1183–1186.

Jennings, J.H., Kim, C.K., Marshel, J.H., Raffiee, M., Ye, L., Quirin, S., Pak, S., Ramakrishnan, C., and Deisseroth, K. (2019). Interacting neural ensembles in orbitofrontal cortex for social and feeding behaviour. Nature *565*, 645–649.

Jiang, B., Huang, S., de Pasquale, R., Millman, D., Song, L., Lee, H.-K., Tsumoto, T., and Kirkwood, A. (2010). The maturation of GABAergic transmission in visual cortex requires endocannabinoid-mediated LTD of inhibitory inputs during a critical period. Neuron *66*, 248–259.

Johnson, P.M., and Kenny, P.J. (2010). Dopamine D2 receptors in addiction-like reward dysfunction and compulsive eating in obese rats. Nat. Neurosci. *13*, 635–641.

Khani, A., Kermani, M., Hesam, S., Haghparast, A., Argandoña, E.G., and Rainer, G. (2015). Activation of cannabinoid system in anterior cingulate cortex and orbitofrontal cortex modulates cost-benefit decision making. Psychopharmacology (Berl.) *232*, 2097–2112.

Kupchik, Y.M., Moussawi, K., Tang, X.-C., Wang, X., Kalivas, B.C., Kolokithas, R., Ogburn, K.B., and Kalivas, P.W. (2012). The effect of N-acetylcysteine in the nucleus accumbens on neurotransmission and relapse to cocaine. Biol. Psychiatry *71*, 978–986.

Lauderback, C.M., Hackett, J.M., Huang, F.F., Keller, J.N., Szweda, L.I., Markesbery, W.R., and Butterfield, D.A. (2001). The glial glutamate transporter, GLT-1, is oxidatively modified by 4-hydroxy-2-nonenal in the Alzheimer's disease brain: the role of Abeta1-42. J. Neurochem. *78*, 413–416.

Linehan, V., Fang, L.Z., and Hirasawa, M. (2018). Short-term high-fat diet primes excitatory synapses for long-term depression in orexin neurons. J. Physiol. *596*, 305–316.

Lowe, C.J., Reichelt, A.C., and Hall, P.A. (2019). The Prefrontal Cortex and Obesity: A Health Neuroscience Perspective. Trends Cogn. Sci. *23*, 349–361.

Massa, F., Mancini, G., Schmidt, H., Steindel, F., Mackie, K., Angioni, C., Oliet, S.H.R., Geisslinger, G., and Lutz, B. (2010). Alterations in the hippocampal endocannabinoid system in diet-induced obese mice. J. Neurosci. *30*, 6273–6281.

Matikainen-Ankney, B.A., and Kravitz, A.V. (2018). Persistent effects of obesity: a neuroplasticity hypothesis. Ann. N Y Acad. Sci. *1428*, 221–239.

Meyer, N., Richter, N., Fan, Z., Siemonsmeier, G., Pivneva, T., Jordan, P., Steinhäuser, C., Semtner, M., Nolte, C., and Kettenmann, H. (2018). Oligodendrocytes in the Mouse Corpus Callosum Maintain Axonal Function by Delivery of Glucose. Cell Rep. *22*, 2383–2394.

Moussawi, K., Pacchioni, A., Moran, M., Olive, M.F., Gass, J.T., Lavin, A., and Kalivas, P.W. (2009). N-Acetylcysteine reverses cocaine-induced metaplasticity. Nat. Neurosci. *12*, 182–189.

Murphy-Royal, C., Dupuis, J.P., Varela, J.A., Panatier, A., Pinson, B., Baufreton, J., Groc, L., and Oliet, S.H.R. (2015). Surface diffusion of astrocytic glutamate transporters shapes synaptic transmission. Nat. Neurosci. *18*, 219–226.

Oliet, S.H., Piet, R., and Poulain, D.A. (2001). Control of glutamate clearance and synaptic efficacy by glial coverage of neurons. Science *292*, 923–926.

Ongür, D., and Price, J.L. (2000). The organization of networks within the orbital and medial prefrontal cortex of rats, monkeys and humans. Cereb. Cortex *10*, 206–219.

Pannasch, U., Freche, D., Dallérac, G., Ghézali, G., Escartin, C., Ezan, P., Cohen-Salmon, M., Benchenane, K., Abudara, V., Dufour, A., et al. (2014). Connexin 30 sets synaptic strength by controlling astroglial synapse invasion. Nat. Neurosci. *17*, 549–558.

Papouin, T., Dunphy, J., Tolman, M., Foley, J.C., and Haydon, P.G. (2017). Astrocytic control of synaptic function. Philos. Trans. R. Soc. Lond. B Biol. Sci. *372*, 20160154.

Reissner, K.J., Gipson, C.D., Tran, P.K., Knackstedt, L.A., Scofield, M.D., and Kalivas, P.W. (2015). Glutamate transporter GLT-1 mediates N-acetylcysteine inhibition of cocaine reinstatement. Addict. Biol. *20*, 316–323.

Rolls, B.J., Rowe, E.A., and Turner, R.C. (1980). Persistent obesity in rats following a period of consumption of a mixed, high energy diet. J. Physiol. *298*, 415–427.

Rubino, T., Realini, N., Braida, D., Guidi, S., Capurro, V., Viganò, D., Guidali, C., Pinter, M., Sala, M., Bartesaghi, R., and Parolaro, D. (2009). Changes in hippocampal morphology and neuroplasticity induced by adolescent THC treatment are associated with cognitive impairment in adulthood. Hippocampus *19*, 763–772.

Seabrook, L.T., and Borgland, S.L. (2020). The orbitofrontal cortex, food intake and obesity. J. Psychiatry Neurosci. *45*, 304–312.

Spiegelman, B.M., and Flier, J.S. (2001). Obesity and the regulation of energy balance. Cell *104*, 531–543.

Tanaka, K., Watase, K., Manabe, T., Yamada, K., Watanabe, M., Takahashi, K., Iwama, H., Nishikawa, T., Ichihara, N., Kikuchi, T., et al. (1997). Epilepsy and exacerbation of brain injury in mice lacking the glutamate transporter GLT-1. Science *276*, 1699–1702.

Thaler, J.P., Yi, C.-X., Schur, E.A., Guyenet, S.J., Hwang, B.H., Dietrich, M.O., Zhao, X., Sarruf, D.A., Izgur, V., Maravilla, K.R., et al. (2012). Obesity is associated with hypothalamic injury in rodents and humans. J. Clin. Invest. *122*, 153–162.

Thoeni, S., Loureiro, M., O'Connor, E.C., and Lüscher, C. (2020). Depression of Accumbal to Lateral Hypothalamic Synapses Gates Overeating. Neuron *107*, 158–172.e4.

Thompson, J.L., Drysdale, M., Baimel, C., Kaur, M., MacGowan, T., Pitman, K.A., and Borgland, S.L. (2017). Obesity-Induced Structural and Neuronal Plasticity in the Lateral Orbitofrontal Cortex. Neuropsychopharmacology *42*, 1480–1490.

Tsai, S.F., Chen, Y.W., and Kuo, Y.M. (2018). High-fat diet reduces the hippocampal content level of lactate which is correlated with the expression of glial glutamate transporters. Neurosci. Lett. *662*, 142–146.

Valladolid-Acebes, I., Merino, B., Principato, A., Fole, A., Barbas, C., Lorenzo, M.P., García, A., Del Olmo, N., Ruiz-Gayo, M., and Cano, V. (2012). High-fat diets induce changes in hippocampal glutamate metabolism and neurotransmission. Am. J. Physiol. Endocrinol. Metab. *302*, E396–E402.

Voutsinos-Porche, B., Knott, G., Tanaka, K., Quairiaux, C., Welker, E., and Bonvento, G. (2003). Glial glutamate transporters and maturation of the mouse somatosensory cortex. Cereb. Cortex *13*, 1110–1121.

Zhang, Y., Reichel, J.M., Han, C., Zuniga-Hertz, J.P., and Cai, D. (2017). Astrocytic Process Plasticity and IKKβ/NF-κB in Central Control of Blood Glucose, Blood Pressure, and Body Weight. Cell Metab. *25*, 1091–1102.e4.

Zhao, L., Yeh, M.L.-W., and Levine, E.S. (2015). Role for Endogenous BDNF in Endocannabinoid-Mediated Long-Term Depression at Neocortical Inhibitory Synapses. eNeuro *2*, ENEURO.0029-14.2015.

STAR★METHODS

KEY RESOURCES TABLE

REAGENT or RESOURCE	SOURCE	IDENTIFIER
Chemicals, peptides, and recombinant proteins		
NMDG	Fisher Scientific	Cat# 6284-40-8
KCl	Fisher Scientific	Cat# P330
NaH2PO4.2H2O	Fisher Scientific	Cat# S369
$NaHCO_3$	Fisher Scientific	Cat# 144-55-8
HEPES	Sigma	Cat# 7365-45-9
D-Glucose	Sigma	Cat# G8270
Sodium Ascorbate	Sigma	Cat# 134-03-02
Sodium Pyruvate	Sigma	Cat# 113-24-6
Thiourea	Sigma	Cat# T8656
$MgSO_4.7H_2O$	Fisher Scientific	Cat# M63
CaCl2.2H2O	Fisher Scientific	Cat# C79
Cesium Methanesulfonate	Sigma	Cat# C1426
CsCl	Sigma	Cat# 203025
Potassium D-Gluconate	Sigma	Cat# G4500
KCl	Fisher Scientific	Cat# P330
HEPES	Sigma	Cat# H3375
EGTA	Sigma	Cat# E3889
Sodium creatine phosphate	Sigma	Cat# 27920
Adenosine 5′-triphosphate magnesium salt (MgATP)	Sigma	Cat# A9187
Guanosine 5′-diphosphate sodium salt (NaGTP)	Sigma	Cat# G7127
QX-314 Chloride	Alomone Labs	Cat# Q-150
D-AP5	Tocris	Cat# 0106
Picrotoxin	Sigma	Cat# P1675
DNQX disodium salt	Hello Bio	Cat# HB0262
Strychnine hydrochloride	Sigma	Cat# 1421-86-9
Tetrodotoxin Citrate	Alomone Labs	Cat# T-550
(RS)-MCPG	Tocris	Cat# 0336
WIN 55,212-2 mesylate	Tocris	Cat# 1038
NESS-0327	Cayman Chemicals	Cat# 10004184
(S)-3,5-DHPG	Tocris	Cat# 0342
MTEP hydrochloride	Tocris	Cat# 2921
γ-DGG	Tocris	Cat# 0112
DL-TBOA	Tocris	Cat# 1223
LY379268 disodium salt	Tocris	Cat# 5064
LY341495	Tocris	Cat# 1209
Sulforhodamine 101	Sigma	Cat# S7635
Rubi-Glutamate	Hello Bio	Cat# HB0567
Fluorescein isothiocyanate(FITC)–dextran (mol. wt. 2,000,000)	Sigma	Cat# 60842-46-8
N-Acetylcysteine	Sigma	Cat#A7250
rabbit-anti-GLT-1	Cell Signaling	3838
RIPA buffer	Thermo Scientific	89900

(*Continued on next page*)

Continued

REAGENT or RESOURCE	SOURCE	IDENTIFIER
cOmplete Protease Inhibitor Cocktail	Roche	11836170001
PhosSTOP	Roche	4906845001
Pierce BCA Protein Assay Kit	Thermo Scientific	23225
mouse beta-actin	GenScript	Cat# A00730, RRID:AB_914100
Goat anti-mouse IgG	Thermo Fisher Scientific	Cat# 31460, RRID:AB_1090267
Experimental models: organisms/strains		
Long Evans Rats (Male) Crl:LE	Charles River	Strain code: 006
Software and algorithms		
pClamp10	Molecular Devices	https://www.moleculardevices.com/
Mini Analysis 6.0.3	Synaptosoft	http://www.synaptosoft.com/MiniAnalysis/
Prism 9	GraphPad	https://www.graphpad.com/

RESOURCE AVAILABILITY

Lead contact

Further information and requests for resources and reagents should be directed to and will be fulfilled by the lead contact, Stephanie L. Borgland, (s.borgland@ucalgary.ca).

Materials availability

This study did not generate new unique reagents.

Data and code availability

- Data are available upon request.
- This paper does not report original code
- Any additional information required to reanalyze the data reported in this paper is available from the lead contact upon request.

EXPERIMENTAL MODEL AND SUBJECT DETAILS

All experiments on rats were approved by the Animal Care Committee of the University of Calgary, under guidelines set by the Canadian Council on Animal Care. Male Long-Evans rats (P50-55) were obtained from Charles River Laboratories and were individually housed in cages with paper bedding (Alphapads, Lawrenceville, GA) on a 12:12 reverse light dark cycle (lights on at 8:00 am).

METHOD DETAILS

Location

This research was performed at the University of Calgary which is located on the unceded traditional territories of the people of the Treaty 7 region in Southern Alberta, which includes the Blackfoot Confederacy (including the Siksika, Piikuni, Kainai First Nations), the Tsuut'ina, and the Stoney Nakoda (including the Chiniki, Bearspaw, and Wesley First Nations). The City of Calgary is also home to Metis Nation of Alberta, Region III.

Diets

In addition to *ad libitum* chow and water, rats were given access to a cafeteria diet (Kraft™ smooth peanut butter, chocolate Timbit™ donut holes, Kirkland™ beef hotdogs, Froot Loops™, Doritos™) for either 24 h per day (Extended access), 1 h per day (Restricted access) or 0 h per day (Chow only) for 40 consecutive days. Energy density and macronutrient composition is listed in Table S1. Rats with restricted access to the cafeteria diet were given their 1 h access to cafeteria diet ~2 h into their dark cycle in addition to 24h access to chow. This restricted access group served as a pair fed control, in which animals had access to the cafeteria diet, but their ability to consume the diet was limited by a short duration of exposure (Ellacott et al., 2010). Rats' body weights were measured before and after 40 days of exposure to the cafeteria diet.

Slice preparation

Rats were deeply anaesthetized with isoflurane and intracardially perfused with N-methyl D-glucamine (NMDG) solution of composition (in mM): 93 NMDG, 2.5 KCl, 1.2 $NaH_2PO_4.H_2O$, 30 $NaHCO_3$, 20 HEPES, 25 D-glucose, 5 sodium ascorbate, 3 sodium pyruvate, 2 thiourea, 10 $MgSO_4.7H_2O$, 0.5 $CaCl_2.2H_2O$. Rats were then decapitated and coronal sections (300 μm) containing orbitofrontal cortex (OFC) were cut in NMDG solution using a vibratome (VT1200, Leica Microsystems, Nussloch, Germany). Slices were recovered in warm NMDG solution (32°C) for 10-12 min before being transferred to a holding chamber containing artificial cerebrospinal fluid (ACSF) of composition (in mM): 126 NaCl, 1.6 KCl, 1.1 NaH_2PO_4, 1.4 $MgCl_2$, 2.4 $CaCl_2$, 26 $NaHCO_3$, 11 glucose (32°C); equilibrated with 95% O2 / 5% CO_2.

Neuronal Electrophysiology

Slices were transferred to a chamber on an upright microscope (Olympus BX51WI) and continuously superfused with ACSF (2 $mL.min^{-1}$, 34°C). OFC neurons were visualized with a 40X water immersion objective using Dodt gradient contrast optics.

Whole-cell voltage-clamp recordings (holding potential = −70 mV) of synaptic currents were made using a MultiClamp 700B amplifier (Axon Instruments, Molecular Devices). Pyramidal neurons in layer II/III of the lateral OFC (~100-300 μm above the inflection point of the rhinal sulcus) were identified by morphological and electrophysiological characteristics (triangular shape, capacitance > 100 pF, input resistance < 100 mOhm). For recording of inhibitory postsynaptic currents (IPSCs), recordings were obtained with an internal solution of the following composition (in mM): 80 $CsCH_3SO_3$, 60 CsCl, 10 HEPES, 0.2 EGTA, 1 $MgCl_2$, 2 MgATP, 0.3 NaGTP, 5 QX-314-Cl (pH 7.2–7.3, 305 mOsm). Inhibitory postsynaptic currents (IPSCs) were pharmacologically isolated with the α-amino-3-hydroxy-5 methyl-4-isoxazolepropionic acid (AMPA)/kainate receptor antagonist, DNQX (10 μM) and the glycine receptor antagonist, strychnine (1 μM). For recording of excitatory postsynaptic currents (EPSCs), recordings were made using an internal solution containing (in mM): 139 $CsCH_3SO_3$, 8 CsCl, 10 HEPES, 0.25 EGTA, 4 MgATP, 0.3 NaGTP, 7 Na-phosphocreatine (pH 7.2–7.3, 305 mOsm). EPSCs were pharmacologically isolated with the $GABA_A$ receptor antagonist, picrotoxin (100 μM) and strychnine (1 μM). Series resistance (5-20 MΩ) and input resistance were monitored online with a 10 mV voltage step given 400 ms every stimulus. IPSCs and EPSCs were filtered at 2 kHz, digitized at 10 kHz and collected using pCLAMP 10 software. In the majority of experiments, electrically-evoked currents were elicited using a bipolar tungsten stimulating electrode (FHC, Maine, USA) placed ~50-300 μm laterally from the recorded neuron. NMDA EPSCs were isolated by recording at +40 mV in the presence of DNQX (10 μM), picrotoxin (100 μM) and strychnine (1 μM). To activate extrasynaptic NMDA receptors, a high-frequency stimulation train of 5 pulses @100 Hz is used to elicit excess glutamate spillover into the extrasynaptic space, which is reflected as a prolongation in the decay time of pharmacologically isolated NMDA eEPSCs. The effect of the glutamate transporter blocker, TBOA (30 μM, 10 min) was then examined on this measure. Half-decay time of NMDA eEPSCs is measured during an initial baseline period (1 min) immediately following whole-cell access to a lOFC pyramidal neuron. AMPA EPSCs were isolated by recording at −70 mV in the presence of picrotoxin (100 μM). Theta-burst stimulation (TBS) consisted of 8 theta-burst trains. Each train contained 10 bursts (200 ms interburst interval), with each burst consisting of 5 stimuli at 100 Hz. Example traces of evoked EPSCs or IPSCs were constructed from averages of 30 sweeps. In a subset of experiments, spontaneous miniature EPSCs or mIPSCs were recorded in the presence of the sodium channel blocker, tetrodotoxin (TTX, 0.5 μM) to inhibit action-potential dependent activity. Individual quantal events were selected based on amplitude (> 10 pA), decay time (< 10 ms) and rise time (< 4 ms) and analyzed using Minianalysis (Synaptosoft).

Astrocyte electrophysiology

Following tissue slicing and recovery, slices were transferred to a temporary holding chamber containing ACSF at physiological temperature and treated with sulfurhodamine-101 dye (SR101, 20 μM, 20 min) uptake by astrocytes. Slices were then transferred back to a regular ACSF holding solution for at least 30 min. For electrophysiology experiments, SR-101-labeled OFC astrocytes were patch-clamped with a glass electrode (~4-5 mΩ) containing internal solution of the following composition (in mM): 130 K-Gluconate, 10 KCl, 10 HEPES, 0.5 EGTA, 10 Na-phosphocreatine, 4 MgATP, 0.3 NaGTP. In addition to SR-101 labeling, astrocytes were confirmed by their small soma size (~10 μm), low resting membrane potential (< −80 mV), low input resistance (< 10 mΩ), passive membrane properties (linear current-voltage (IV) relationship) and a lack of action potential firing. These properties distinguish astrocytes from oligodendrocytes, which have a higher input resistance of ~60 mΩ (Meyer et al., 2018). Astrocytes were recorded in voltage-clamp configuration (−80 mV) in the presence of the following synaptic blockers: DNQX (10 μM), picrotoxin (100 μM), strychnine (1 μM), the N-methyl-d-aspartate (NMDA) receptor antagonist, D-AP5 (50 μM) and the non-selective Group I/II metabotropic glutamate receptor antagonist, MCPG (250 μM). Glutamate was applied onto astrocytes by uncaging Rubi-glutamate via flash photolysis (473 nm, 2 ms, Thorlabs). At the conclusion of each recording, the glutamate transport blocker, TBOA (30 μM) was finally added to abolish the recorded current. Remaining residual currents were subtracted from the original response to specifically isolate a glutamate transporter current.

Astrocyte Dye-filling

OFC astrocytes located at a depth of ~20-50 μM from the slice surface were patch-clamped with an internal solution of the following composition (in mM): 108 K-gluconate, 8 Na-gluconate, 2 $MgCl_2$, 10 HEPES, 1 K_2-EGTA, 4 K_2-ATP, and 0.3 Na_3-GTP. Once a gigaΩ seal was observed, whole-cell configuration was obtained to initiate filling of astrocytes with Dextran-FITC (3-5 kDa) dye. Access resistance was maintained below 20 MΩ throughout the experiment. Cells were allowed to fill for a minimum

of 10 min before z stack, allowing visualization of the full morphology of individual astrocytes. Astrocytes were identified by their SR101 dye uptake, presence of vascular endfeet (observed following FITC-dextran loading) and low input resistance (10-20 MΩ). Fluorescence imaging was performed on a custom two-photon laser-scanning microscope optimized for acute brain slices and patch-clamp electrophysiology. The microscope was equipped with a Ti:Sapph laser (Ultra II, ~4 W average power, 670–1080 nm, Coherent), objectives (Zeiss 40 × NA 1.0, Nikon 16 × NA 0.8), a green bandpass emission filter (525–40 nm), an orange/red bandpass emission filter (605–70 nm), and associated photomultiplier tubes (GaAsP Hamamatsu). Z stacks were used to assess the extent of FITC-dextran (3-5kDa) diffusion in individual astrocytes. To image FITC-dextran during astrocyte filling, the Ti:Sapph laser was tuned to 800 nm.

Western Blot Analysis

Western blot analysis for GLT-1 was performed on samples of OFC dissected from 100 μm thick frozen sections. Samples were homogenized and sonicated in ice-cold RIPA buffer (Thermo Scientific, 89900) with cOmplete Protease Inhibitor Cocktail (Roche, 11836170001) and PhosSTOP (Roche, 4906845001). The homogenate was centrifuged at 13,000 ***g*** for 20 min at 4°C. The supernatant was collected and protein content was measured using a Pierce BCA Protein Assay Kit (Thermo Scientific, 23225). The samples were denatured with a loading buffer containing 2-mercaptoethanol for 20 minutes at room temperate then the mixture (20 μg/lane) was loaded onto a 10% sodium dodecyl sulfate-polyacrylamide gel electrophoresis (PAGE) gel and run on a minigel system (Bio--Rad., Mississauga, ON, Canada). After the protein was transferred to PVDF membrane following electrophoresis, the membrane was blocked in 5% milk followed by the incubation with rabbit anti GLT-1 (Cell Signaling, 3838) at 1:250 at 4°C for 24 hours. For loading control, mouse beta-actin (GenScript Cat# A00730; RRID:AB_914100) at 1:2500 was applied at room temperature for 1 hour. The blots were further incubated at room temperature for 1 h with horseradish peroxidase-conjugated goat anti-rabbit IgG 1:2500 for GLT-1 or goat anti-mouse IgG 1:2500 for beta-actin (Thermo Scientific, 31460 and 31430). Finally, antibody binding was visualized using the enhanced chemiluminescence (ECL) system (Thermo Scientific, 32109) and scanned with a Gel Doc system (Bio-Rad, Mississauga, ON, Canada). The band density of GLT-1 (MW 65 kDa) was analyzed with ImageJ and normalized against the loading control.

Immunohistochemistry

Coronal sections containing the OFC were incubated with blocking solution (5% goat serum, 1% BSA, 0.5% Triton X-100 in 0.1 M PBS) to prevent nonspecific binding. Floating sections were incubated in primary antibody GFAP (1:1000; MAB360, Millipore) overnight at 4°C, washed, and then incubated with secondary antibody (goat anti- rabbit, 1: 500) labeled with Alexa Fluor 488 for 1 h at room temperature. Slices were then mounted on Superfrost Plus clear slides (VWR international), dried, coated with Fluromount medium (Diagnostic Biosystems, Pleasanton, CA, USA) and coverslipped for imaging. Confocal fluorescent images were collected using Nikon Eclipse C1si spectral confocal microscope with motorized stage (Nikon Canada Inc., Ontario, CANADA). The objectives used were 10x PLAN APO DIC (NA 0.45), 20X PLAN APO DIC (NA 0.75) and 60x PLAN APO water immersion DIC (NA 1.20). The laser used was centered at 488 nm (with 515/30 emission filter) wavelengths for detecting GFAP. Threshold levels were adjusted to 20 (min) to 225 (max) pixels and particle analysis was based on size restriction of 0 cm^2 to infinity. All the images were employed the same settings to be consistent for image analysis.

Four coronal slices from the OFC were taken from 5 rats per group. Within each slice, four non-overlapping images per brain region were imaged for a total of 16 images per brain region of a given animal. A total of 80 fields of view were captured per animal at 60x magnification for GFAP staining. All the images were taken using imaging software EZ C1 for Nikon Confocal, Silver Version 3.91 (Nikon, Canada Inc., Ontario, CANADA). Stacked images were acquired using two frames with a resolution of 512x512 pixels. Offline image processing included maximal intensity projections was conducted using NIS elements. Fluorescence intensity (intensity units, IU) and percentage area of fluorescence was quantified for each image using ImageJ (1.48v, Wayne Rasband, National Institute of Health, USA). All images were taken blinded to the treatment of the rats.

QUANTIFICATION AND STATISTICAL ANALYSIS

All statistical analyses were performed in GraphPad Prism 7.02 (GraphPad, US). A two-way repeated-measures analysis of variance (RM-ANOVA) was used to examine effects of two factors between multiple groups. With time course data, some cells died before the end of recording and therefore matching on every point could not be achieved, therefore we used a mixed-effect model (REML) repeated-measures two-way ANOVA. A one-way ANOVA was used to compare the effect of a treatment between multiple groups. Unless otherwise indicated, a Tukey's multiple comparison test was used to assess within group differences. A two-sample t test was used to compare between two groups when normality distribution was assumed. A one sampled t test was used to assess difference from 100%. Significance was set at $p < 0.05$. A Shapiro-Wilk test was used to assess for normal distribution of data. All data are expressed as mean ± standard error of the mean (SEM). Individual responses are plotted over averaged responses. Experimental designs and samples sizes aimed at minimizing usage and distress of rats, and were sufficient for detecting robust effect sizes. N refers to number of rats whereas n refers to number of cells/number of rats.